3 Block Copolymers and Graft Copolymers

3.1 General Introduction

Homopolymers consist of one kind of repeating unit throughout the whole backbone strand. These structurally simple polymers constitute by far the largest share among plastics and already show great diversity and adaptability to required applications depending on the nature of their repeating units as well as their molecular weight and weight distribution. But the freedom of design is greatly expanded not only by incorporating structurally different repeating units into a given polymer strand but also by manipulating their ratio and position in the backbone sequence. These possibilities give rise to a number of copolymer classes including (i) random copolymers possessing an arbitrary heterosequence, (ii) alternating copolymers with strictly alternating repeating units, (iii) block copolymers consisting of two or more segments of pure homosequences, and (iv) graft copolymers in which polymeric side chains of one repeating unit are grafted to a strand of another repeating unit, among others (Figure 1).

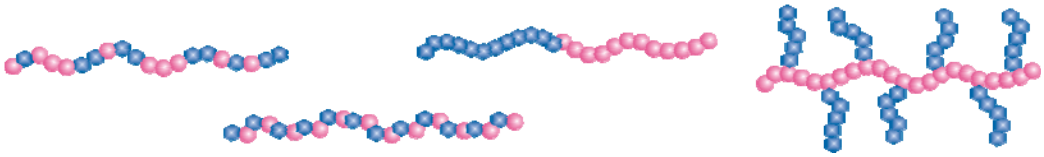

Figure 1: Different copolymer architectures: random copolymer, alternating copolymer, block copolymer, and grafted copolymer (from left to right).

Meshing characteristics of often-complementary homopolymers into a single block copolymer strand is not comparable to the mere blending of homopolymers and opens the access to novel properties not found in either homopolymer, often arising from the possibility of microsegregation of segments[1] or chirality and solubility transfers.[2] This microscopic phase separation leads to the generation of manifold morphologies in the bulk tunable by often competing interactions between the different segments,[3] and thus provide an attractive non-lithographic route to nanostructures.[4] Depending on the flexibility of the segments, coil-coil and rod-coil block copolymers are distinguished, the latter possessing a rigid and hardly flexible rod-like segment. While the assembly characteristics of coil-coil copolymers are mainly governed by microphase-separation, the disparity of stiffness among rod-coil copolymers leads to a selective aggregation with high structural order or even crystallization of the rod-like segments, often dominating the self-assembly[5] while the flexible coil acts as separator between the ordered phases.

Biological-synthetic hybrid block copolymers[6] significantly improve the interactions between man-made nanoobjects and biology, i.e. biomolecules, and may find application in as diverse fields as biosensors,[7] therapeutics, or biomineralization.[8] At the same time, the inherent structural information in many biological macromolecules can be merged together with synthetic macromolecules into a hybrid material to precisely arrange and assemble artificial functional moieties or form accurately shaped nanoobjects of defined dimensions.[6, 9] It should be pointed out, that the mere synthesis of an amino acid sequence on a solid or soluble polymeric support,[10] as discussed in Chapter 2, already generates by itself a block-copolymer.

Controlled aggregation of linear amphiphilic block copolymers results in hierarchical structured aggregates based on their amphiphilicity and the proportions, i. e. aspect ratio, of their individual components, and the overall dimensions are much larger than among small molecule assemblies. Formation of helical fibers, coiled ribbons, and tubules is a common motif in the assembly of lamellar sheets among chiral block copolymers. Micelles of a spherical or cylindrical shape[11] represent another possibility to assemble into discrete nanoobjects.

Of special interest are copolymers containing π-conjugated segments. Conjugated polymers often show poor solubilities due to their inherent stiffness and low flexibility as well as to a strong tendency to self-aggregate, further facilitating undesired precipitation. This aggregation in solution and crystallization in films dramatically affects optical and electrical properties, as π-π-interactions between packed backbones alter absorption and conduction behavior, and quench emission. Several approaches for solving these problems are imaginable, one of them being the incorporation of the conjugated polymer into a block copolymer possessing one or more segments of a flexible polymer strand with high solubilizing power. Flexible segments in block copolymers not only increase overall solubility, but also “dilute” the functional conjugated segments and reduce intermolecular contact and aggregation. These hybrid materials exhibit great potential for (opto)electronic applications.

Stimuli-sensitive self-assembled materials constitute an increasingly interesting research field. In this case, an external induction of supramolecular reorganization in the bulk, i. e. phase segregation, directly translates into switching macroscopic properties, e.g. temperature-proton conductivity changes among coil-coil diblock copolymers.[12] A more sophisticated approach relies on the controlled and reversible change of aspect ratio of a given nanostructure and allows for intriguing possibilities of function and application. For example, Jenekhe and coworkers designed a triblock copolymer consisting of a central polyfluorene

segment between two polyglutamate peptide segments.[13] The peptide segments can undergo solvent-induced conformational transitions between a rod-like α-helix and a random coil and then the copolymer can follow different assembly pathways forming lamellar and spherical surface patterns, respectively as observed by AFM. Similarly, artificial helices such as *meta*-phenylene ethynylenes may assume the role of the "switchable" segment and this concept is presented in Section 3.4.5.

3.2 PEG-block-PmPE Copolymers

The experience gained from the *o*PE-oligomer synthesis on a soluble support is the basis to a first exploratory attempt to block copolymers. As the poly(ethylene glycol) (PEG) from Section 2.6.6 is bifunctional, a triblock copolymer was envisioned consisting of a central flexible and solubilizing PEG segment and two poly(phenylene ethynylene) segments attached to it. All needed reaction steps such as anchoring on PEG and Sonogashira couplings as well as isolation and purification of those materials were already tested and optimized.

Thus, PEG **29** with an M_n = 8000 carrying aryl iodides at both termini was submitted to Sonogashira polycondensations with a large excess of *meta*-phenylene ethylene monomer, either still TMS protected (**77**) using the *in-situ* desilylation protocol[14] or carrying the free ethynyl group (**78**) applying standard cross-coupling conditions[15] (Scheme 1). The corresponding GPC results were promising, showing successful polymerization of around 10 r. u. onto the PEG segment.

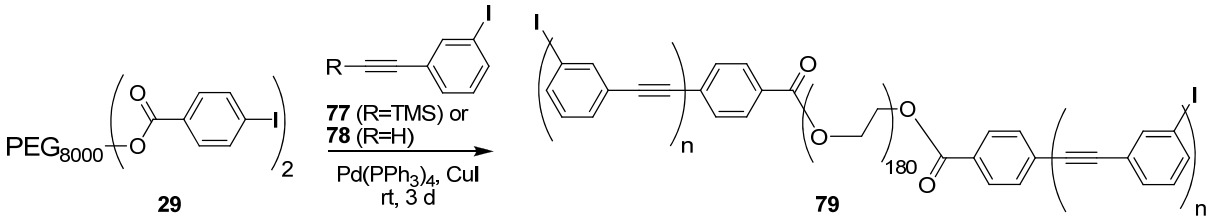

Scheme 1: Generation of a triblock copolymer based on a central poly(ethylene glycol) block activated on both termini, and two poly(meta-phenylene ethynylene) blocks attached to it. Reaction conditions: R = H: in neat Et_3N, 47 %; R = TMS: DBU, H_2O, in toluene or acetonitrile, 84 %.

The next step consisted in finding a more interesting flexible segment than PEG. The required flexible block should be available in different lengths and low polydispersities, be monofunctional, and ideally be chiral. Hereby, a chiral block should be solely consisting of enantiomeric monomer units resulting in a non-racemic polymer. Please note that even highly isotactic PPO exists as a racemic mixture. With these requirements in mind, we decided to synthesize the flexible polymer blocks ourselves, and enantiopure isotactic poly(propylene oxide) (PPO) was chosen as ideal candidate, representing the simplest chiral derivative of PEG. Stereoregular poly(propylene amine)s[16] or poly(propylene sulfide)s[17] (Figure 2)

resemble similar backbones but are less well known, enantiopure monomers are not commercially available or more expensive, and their polymerizations perform inferior to propylene oxide.

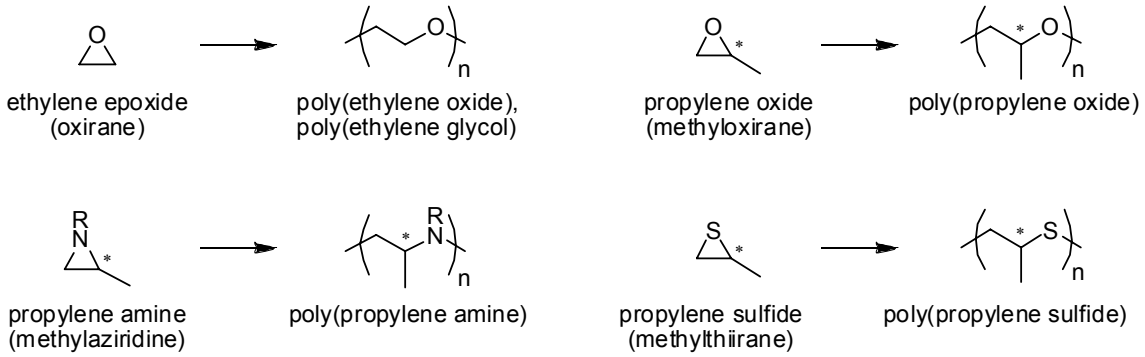

Figure 2: Achiral PEG (top left), chiral analogue PPO (top right) and PPO derivatives based on other heteroatoms (bottom).

3.3 Poly(propylene oxide)s

3.3.1 Introduction

Comparing poly(propylene oxide) with poly(ethylene oxide), one more methyl group per repeating unit changes properties dramatically, e. g. PPO is much less polar. While PEG can be precipitated in ether and cold ethanol, PPO is soluble in everything but water. Furthermore, the additional methyl group generates a chiral center from which tacticity arises. While atactic PPO is a clear colorless oil, isotactic PPO constitutes a white crystalline solid of known crystal structure.[18] Although most commercial polypropylene is isotactic, all commercial PPO is atactic due in part to the high expense of enantiopure propylene oxide (PO) as well as to the lack of suitable catalysts for the stereospecific polymerization of racemic PO.

The simplest ring-opening polymerization of PO uses alkali bases like KOH as initiator for the anionic polymerization. The high basicity of the initiator and the propagating species lead to region-defects such as head-to-head or tail-to-tail formation due to low selectivity in the PO opening. The terminal dehydroxylation constitutes a major termination reaction, generating an allyloxy group and thereby stopping chain growth. Addition of diverse catalysts[19] can reduce these effects. Other initiator-catalyst systems include bis(dialkylaluminum)oxides[20] or dialkylzinc-water adducts.[21] A variety of catalysts and initiators have been developed over time to enable living polymerizations and isotactically enriched PPOs of controlled length and polydispersity, but atactic byproducts could not completely be eliminated. Inoue and coworkers extensively investigated bulky aluminum[22] and zinc[23] porphyrin complexes as initiators and also found an acceleration of the polymerization via activation of the monomer

by Lewis acids.[24] Cationic polymerizations initiated with Lewis acids have also been reported on.[25] An excellent review by Kuran[26] provides an overview on the field of ring-opening polymerizations of heterocyclic monomers. Very recently, Coates reported on a highly isotactic PPO from racemic PO using a homogeneous stereoselective diamine-cobalt complex.[27]

An easy and fast access to controlled anionic polymerizations initiated by alkali metal alkoxide and trialkylaluminum catalysts was reported by Deffieux.[28] No defects in terms of regioinversions and termination reactions were observed while at the same time a good control of chain length at low polydispersities was achieved. As all reagents are commercially available or easy to access, a procedure based on this report was used throughout this work.

Isotactic PPOs are also accessible via polymerization of enantiopure PO,[21, 29] although the reported initiating-catalyzing systems do not prevent partial racemization. These isotactic polymers arising from enantiopure PO display optical activity,[30, 31] as only one possible isotactic strand is generated, e. g. (*S*)-propylene oxide leads to an isotactic backbone of *all*-(*S*)-configuration without any opposing isotactic *all*-(*R*)-strands.

3.3.2 Synthesis and Characterization of PPOs

The synthetic procedure for poly(propylene oxide)s was adopted from the work of Deffieux and coworkers.[28] Benzyl alkoxide, generated by deprotonation of benzyl alcohol with elemental sodium, was chosen as initiator. This initiator, as opposed to metal hydroxides, generates monofunctional polymers, it acts as a UV label during work-up and analysis, and can subsequently be removed by hydrogenolysis followed by post-functionalization. The catalyst tri-isobutylaluminum plays a dual role. It controls the growth and inhibits defects by lowering the basicity of the active chain end and it activates the monomer for an accelerated addition to the propagating chain end by coordination to the PO's oxygen. The proposed mechanism is shown in Scheme 2. The polymerizations were run in heptane-toluene solvent mixtures at 0 °C. The reaction was quenched with acidic ethanol after 3 hours, when all the

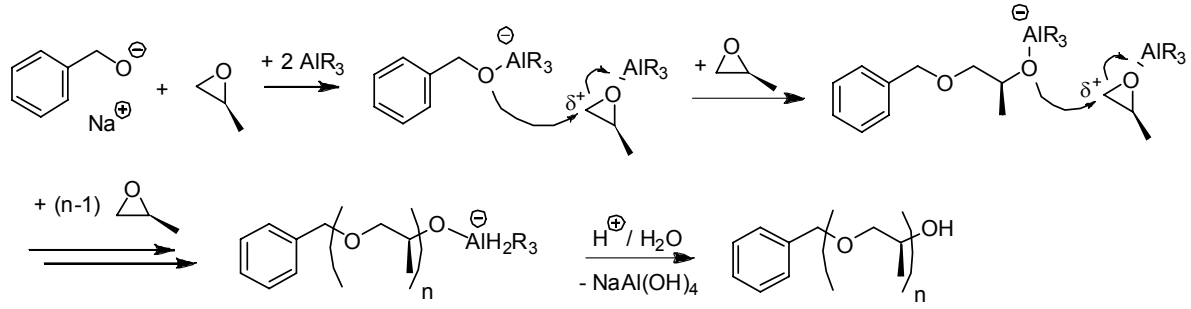

Scheme 2: Proposed polymerization mechanism of enantiopure (S)-propylene oxide to isotactic poly(propylene oxide) with an alkoxide initiator under trialkylaluminum catalysis.

monomer was consumed. The reaction conditions were optimized for the polymerization of racemic PO in terms of control of chain length and polydispersity and selected results for atactic and isotactic PPOs are presented in Table 1. An optimal catalyst:initiator-ratio of 7:1 was chosen.

Purification and fractionation of atactic PPO was only possible by precipitation in water-methanol mixtures. Instead, isotactic PPO and all derivatives could readily be recrystalized from acetone at -20 °C. All PPOs were fully characterized. GPC analysis overestimated the molecular weight, thus chain lengths were determined by ^{1}H-NMR endgroup analysis (Figure 3). The GPC results were used to determine the polydispersity and ^{13}C-NMR was employed to monitor tacticity.

compound	monomer:initiator ratio	catalyst: initiator ratio	theoretical M_n	M_n by GPC	M_n by NMR	PDI
80b-5	196:1	5	11400	35000	-	1.22
80b-7	196:1	7	11400	32000	11300	1.18
80b-9	200:1	9	11600	37000	14800	1.18
80a	69:1	7	4100	17000	5900	1.17
80c	400:1	7	23200	44000	20900	1.23
81a	69:1	7	4100	6500	5300	1.90
81b	200:1	7	11600	27000	12000	1.16
81c	333:1	7	19400	50000	24700	1.25
81d	33:1	5	2000	8300	2900	1.10

*Table 1: Selected polymerization results for atactic PPOs **80** based on racemic PO and isotactic PPOs **81** based on enantiopure (S)-PO.*

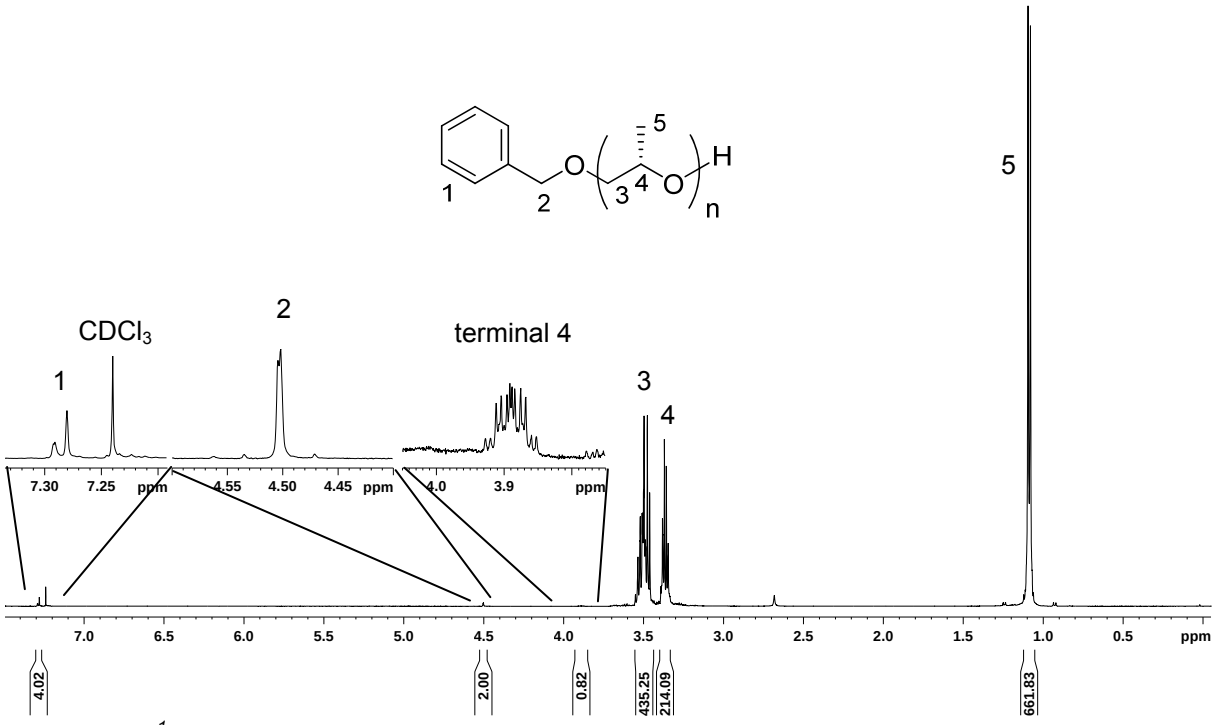

*Figure 3: ^{1}H-NMR spectrum of PPO **81b** in $CDCl_3$. With H-2:H-3 = 2:435 → n = 217, M = 12000.*

Figure 4 shows a comparison between a representative atactic and isotactic PPO NMR-spectrum. While the ^{1}H-NMR spectra only differ in the splitting of the methyl signal, the ^{13}C-NMR spectra display eye-catching differences. In the spectrum of the atactic polymer, even triads and tetrads consisting of all possible stereosequences were assigned,[32] proving the presence of fully atactic material. This is further supported by the observation that no crystalline (i.e. isotactic) material could be precipitated in cold acetone at all. In contrast, the spectrum of isotactic PPO displays a significantly reduced number of signals demonstrating the high degree of isotacticity and absence of regioinversion defects.[33] As PPOs lack UV/vis-active groups, optical spectroscopy is limited by solvent absorbance and spectrometer set-up. A representative absorbance and CD spectrum for the isotactic and optically active PPO **81b** in MeCN is shown in Figure 5. Polyether backbone absorption starts below 220 nm while MeCN enables transmission down to 190 nm. The observed circular dichroism is agreement with the literature.[31] Additional strong CD signals are reported below 190 nm for different solvents.

The influence of the PPO chain length on the properties in the bulk were studied by heating and cooling cycles monitored by DSC. The observed features for poly(propylene oxide)s of chain lengths between M_n = 2000 and M_n = 20000 are similar. The melting on the first heating of the virgin sample is preceded by a shallow endothermic area between around 30 to 55 °C for PPOs **81a** and **81c**. The actual melting starts at 60 °C and shows a peak at 67 - 69 °C, sharply leveling off afterwards (Table 2, Figure 6 shows a representative DSC trace).

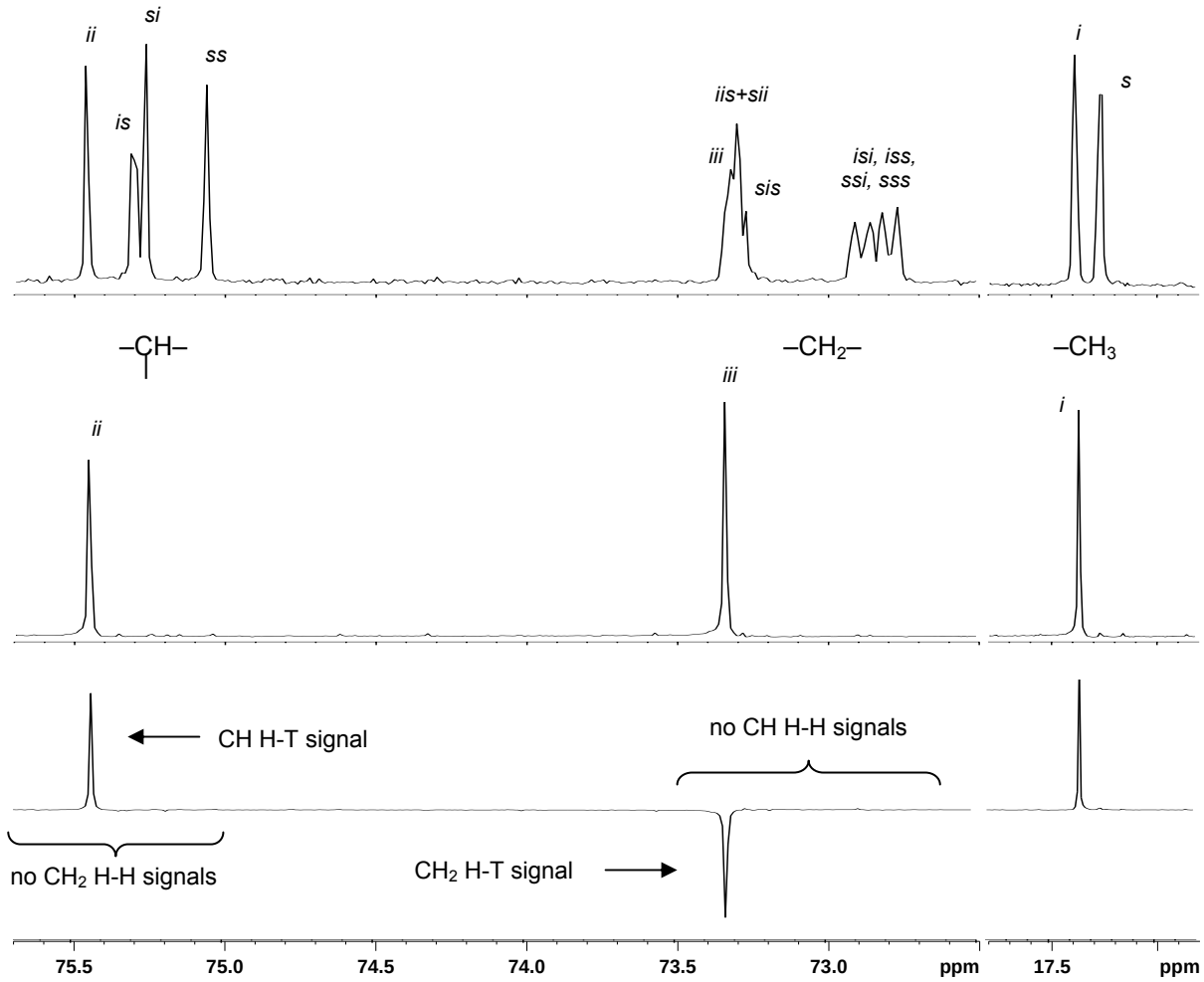

*Figure 4: NMR spectra of PPO in $CDCl_3$ (expansions of relevant regions): ^{13}C-NMR spectrum of atactic **80b** (top) and isotactic **81b** (middle), 135° DEPT NMR spectrum of isotactic PPO **81b** (bottom), i and s refer to isotactic and syndiotactic diads, triads, and tetrads, H-T and H-H to head-to-tail and head-to-head connectivity, respectively.*

The PPO **81d** with an M_n = 2000, resembling more a resin than a crystalline solid, already melts at 55 °C displaying the same pre-melting like other PPOs. The freezing on the cooling cycle appears retarded on all samples and differs among them. PPO **81c** with the longest chains freezes over a temperature range of nearly 50° with an exothermic maximum at 2 °C,

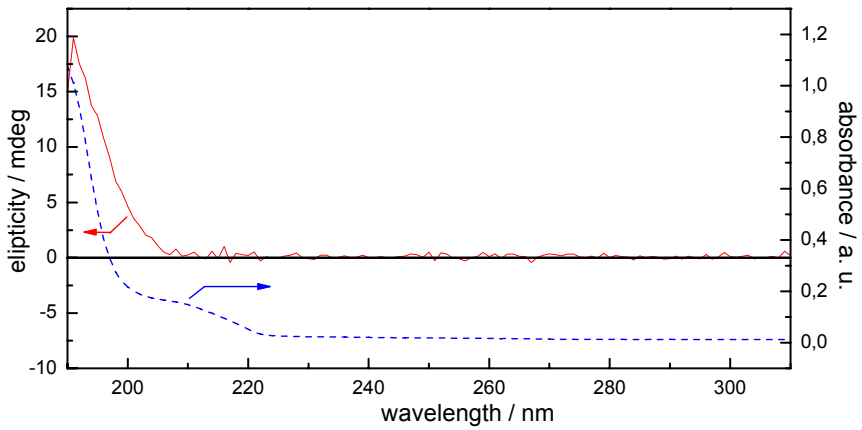

*Figure 5: Absorbance (dashed blue) and CD (solid red) spectrum for isotactic and optically active PPO **81b** in MeCN at 20 °C.*

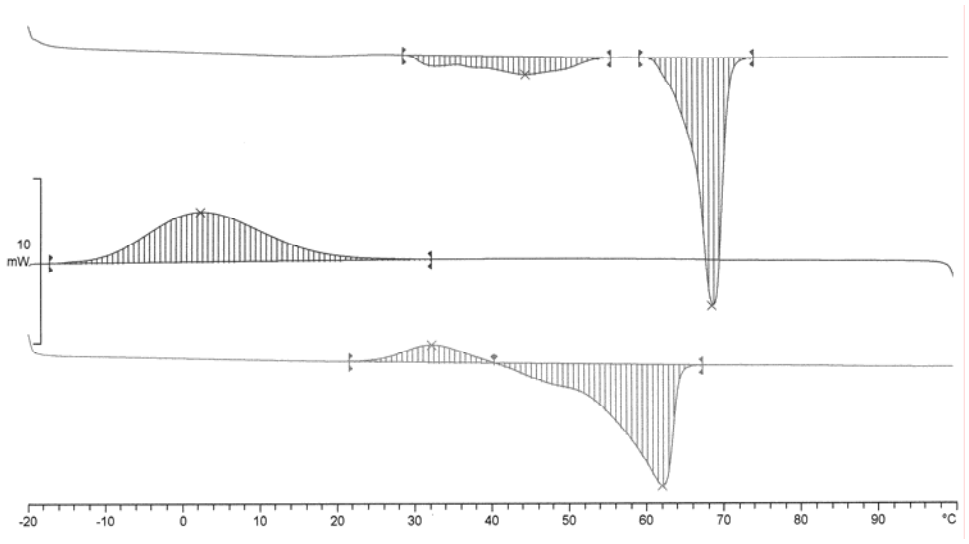

*Figure 6: DSC trace of isotactic non-racemic PPO **81c** (Mn = 20000); from top to bottom: first (virgin) heating, cooling, and second heating under nitrogen atmosphere at a speed of 10 K/min.*

while PPO **81b** freezes quicker between 44 and 20 °C. PPOs **81a** and **81d** freeze in an interval of 32 K and an exothermic peak at 2 °C and 4 °C, respectively. The freezing strongly depends on the cooling rate, as the crystallization of molten samples is kinetically hindered. A temperature ramp of 10 K per minute was set for heating as well as cooling. At the second heating cycle the melting peaks are preceded by an exothermic signal indicating an undefined thermal relaxation in the bulk. The sum of crystallization heat (upon cooling) and exothermic rearrangement (upon second heating) roughly resembles the melting heat during second heating. As crystallization at room temperature takes hours, the forced crystallization upon cooling does not lead to the thermodynamically preferred arrangement in the bulk. Upon cooling to -100 °C, slight glass transitions were observed around -70 °C. Scarce DSC measurements reported in literature were performed on first heating cycle, probably due to the prolonged solidifying process, but confirm melting points around 60 °C.[34] The reported melting heats were much lower as the material was less isotactic.

compound	**81a**	**81b**	**81c**	**81d**	**80b**
M_n	5000	10000	20000	2000	10000
melt peak in °C, 1. heating / 2. heating	66.9 / 59.6	69.3 / 67.9	67.9 / 61.7	54.8 / 54.9	- / -
freeze peak in °C	2.3	26.5	2.4	4.3	-
glass transition in °C, cooling / reheating	-74 / -80	-82 / -70	-65 / -64	-67 / -64	-73 / -70
crystallization heat J/g	51.3	55.1	51.8	54.8	-
exoth. rearrang. J/g	9.1	9.6	9.1	8.9	-
melting heat J/g	-63.9	-61.9	-62.8	-65.2	-

*Table 2: DSC results for isotactic PPOs **81a-d** and atactic **80**.*

A representative DSC measurement was performed with atactic PPO **80b** with a molecular weight of M_n = 10000. Atactic PPOs are oils at room temperature due to their irregular backbones and lack of long-range order. **80b** does not show crystallization upon cooling, just starting at -68 °C a glass transition is observed with a turning point at -73 °C, reappearing upon heating with a turning point at -70 °C and a peak -67 °C.

3.4 Block Copolymers

3.4.1 PPOs in Block Copolymers

Poly(propylene oxide) (PPO) is used in block copolymers as the flexible and solubilizing block segment. The incorporation of PPO blocks into a given rigid polymer allows the tuning of melting and phase-change temperatures alleviating processing and softening the obtained material. PPOs were combined with poly(*para*-benzamide) blocks[35] and also utilized in multi-block copolymers alternating with aliphatic polyamide segments[36] or poly(ethylene terephthalate-co-caprolactone) segments[37] to give thermoplastic elastomers. Furthermore, PPOs have been utilized in block copolymers as flexible coil segments to tune the self-assembly and control the organization in the bulk[38] as described in the introduction. In all of the presented examples commercially available atactic PPOs were used. Although sufficient for mere solubilizing and coil forming purposes, a higher structural order in the backbone itself might prove beneficial.

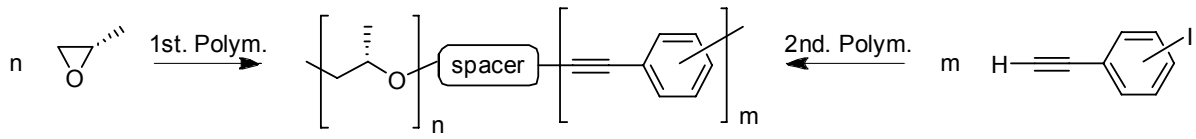

Scheme 3: 3-step approach to rod-coil block copolymers (center) by polymerization of first block, introduction of an adequately functionalized spacer, and polymerization of second block onto it.

Our concept is based on highly isotactic and non-racemic PPO polymerized from enantiopure (*S*)-propylene oxide as the flexible coil block and unsubstituted poly(phenylene ethynylene) as the rigid-rod or switchable block. The use of non-racemic PPO facilitates purification (recrystallization from acetone), improves side chain and enables the possibility of chirality transfer from the PPO block to the aromatic segment and at the same time its monitoring by CD spectroscopy. The block copolymer synthesis starts from carefully prepared PPO segments of controlled lengths and low polydispersities (see preceding Section). Anchoring of a suitable entity onto the PPOs' terminal hydroxyl groups provides the PPO segments for Sonogashira cross-couplings. The second poly(phenylene ethynylene) block will be directly polymerized onto the activated PPO block applying a large excess of

monomer, a procedure resembling the soluble support methodologies. This approach not only promises a quicker access to ready-made block copolymers but is also crucial for generating longer PPE segments, as pre-formed rod segments without solubilizing side chains are severely prone to aggregation and precipitation. The concurrent homopolymerization of PE-monomers in solution resembles a drawback of the approach as considerable amounts of monomer are wasted; however, it should not hamper block copolymer formation and isolation. Lacking solubilizing side chains, longer homopolymers will precipitate off the reaction mixture, and short soluble PE homooligomers should differ enough in their properties from the block copolymers to be separated by, e. g. selectively inducing precipitation of the PPO segments and thus of the block copolymers.

3.4.2 Poly(*para*-Phenylene Ethynylene)s in Block Copolymers

3.4.2.1 Introduction

All PpPE-block copolymers found in the literature are based on substituted phenylene ethynylene repeating units, due to the chosen synthetic approach of synthesizing the blocks individually and then coupling them together as the last step. In addition, solubility and aggregation problems are minimized. For example, Müllen[39] and coworkers synthesized a short P*p*PE with 5 to 6 repeat units each carrying two hexyl side chains and condensed it via an ester function to a PEG (~ 17 r. u.), while the group of Okamoto[40] reported on a triblock copolymer consisting of a central P*p*PE with octyl side chains and two short PEG segments attached to it in order to prevent aggregation when casted as blends with poly(methylmetacrylate)s in thin films. Lazzaroni condensed a short, hexyl-substituted PpPE segment with a poly(dimethylsiloxane) segment to a diblock copolymer.[41] Finally, Tan and coworkers[42] reported on an oligonucleotide-poly(*para*-phenylene ethynylene) block copolymer and have thus far been the only ones to directly polymerize the P*p*PE onto an existing block segment, although with incomplete DNA coverage and with undefined PE chain lengths.

Unsubstituted poly(para-phenylene ethynylene)s are hardly known, as the material becomes completely insoluble when polymerized to lengths exceeding ca. 10 repeat units.[43-45] Yet this structure is specially appealing as it resembles the parent structure of all substituted P*p*PEs[15] and its electronic and optical properties are not biased by electron donating or withdrawing substituents.[46] Very few reports exist on these unsubstituted polymers and no characterization was given due to total insolubility[45, 47] and chain lengths of soluble fractions ranging from 6 to 7 repeat units.[48] Nevertheless, a few examples for short unsubstituted

oligomers – all carrying bulky silyl groups on both termini to increase solubility – can be found, including a mere tetramer and[44] pentamer.[49] The incorporation of an unsubstituted P*p*PE into a block copolymer could overcome intrinsic solubility and aggregation problems and enable the study of lengthier members of this class of conjugated polymers, as the usual solubilizing side chains of known PpPEs would be "outsourced" and merged to a single strand resembling the flexible coil segment of the block copolymer and leaving the naked and now electronically unaltered PpPE backbone as the second block.

A triblock copolymer possessing a non-substituted π-conjugated segment was reported by Stupp and coworkers.[50] Here, a phenylene vinylene hexamer was combined with blocks of polystyrene and polyisoprene differing in length to study aggregation modes.

3.4.2.2 Synthesis of unsubstituted Poly(para-Phenylene Ethynylene) Homopolymers and Block Copolymers

In order to polymerize phenylene ethynylene monomers onto the PPO a suitable functional group on the PPO terminus has to be generated. Adequate functionalities for Sonogashira coupling include aromatic iodides and terminal ethynyl groups. As reasoned in Section 2.6.6, having the halide function on the starting polymer block prevents incorporation of diyne defects into the growing backbone anchored to the first segment. As the present PPO blocks are all hydroxyl-terminated, an ester moiety might serve as linker, and hence *para*-iodobenzoic acid was chosen for activating the PPO terminus towards Sonogashira reactions.

para-Iodobenzoic acid **27** was quantitatively converted into the activated acid chloride **28** with oxalyl chloride and subsequently condensed with PPO strands **81** of different lengths (Scheme 4). The acid chloride was used in 10-fold excess in combination with prolonged reaction times to ensure complete coverage of all PPO strands, as access to their reactive hydroxyl-sites might be kinetically hindered by partial embedment in PPO coils. After aqueous work-up, the obtained activated PPOs **82** were purified by recrystallization from acetone at -20 °C to remove the excess of reagents, and final traces of meanwhile hydrolyzed acid chloride were removed by precipitation in cold dichloromethane. All PPOs and their

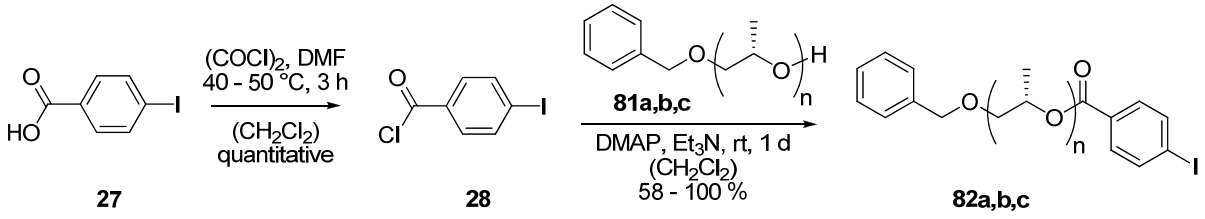

Scheme 4: Activation of para-iodobenzoic acid and its condensation to hydroxyl-terminated PPO polymers to generate activated PPOs for subsequent block copolymer synthesis; a: n = 100, M_n = 5000, b: n = 200, M_n = 10000, and c: n = 400, M_n = 20000.

derivatives that had contact with water or protic polar solvents were further purified by azeotropic concentration of benzene solutions and drying of the solids *in vacuo* for several days. Complete conversion of all hydroxyl-groups was confirmed by endgroup analysis using ^{1}H-NMR. The yield was lowest for the short PPO; probably along the recrystallization steps some material stayed in solution.

The obtained iodoaryl-terminated PPO blocks **82** were reacted with a 100-fold excess of phenylene ethynylene monomer **83** (Scheme 5), which was generated out of the TMS-protected *para*-monomer **85** via TBAF activation. This prolonged Sonogashira polycondensation for generation of the second segment provided the desired diblock copolymers **84a-c**.

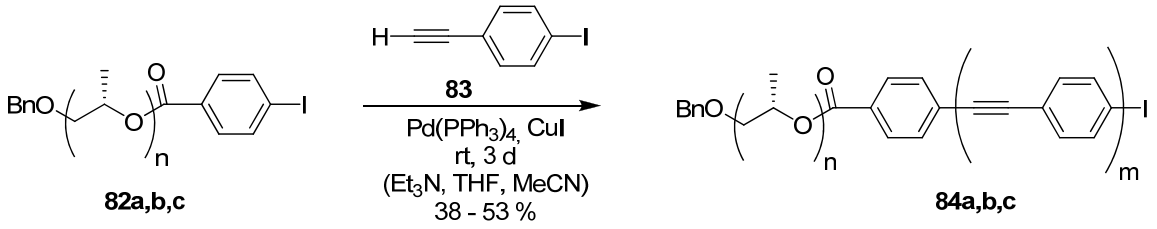

Scheme 5: Polymerization of para-ethynyl-iodobenzene to activated PPOs of different lengths (a: n ≈ 100, Mn = 5000, b: n ≈ 200, Mn = 10000, and c: n ≈ 400, Mn = 20000; m = 10 – 12).

The purification of these crude block copolymers turned out to be tedious. PE-homopolymers aggregated extensively with aromatic segments of block copolymers forming a colloidal suspension, which proved inseparable by simple purification steps. For ^{1}H-NMR determination of PE block lengths (*vide infra*) extremely pure block copolymers were required as homo-PEs and aromatic phosphorous compounds present as impurities gave signals interfering with the PE-block signals. A combination of several purification steps including precipitations, filtrations, recrystallizations, and centrifugations gave non-coloidal material that was further purified by column chromatography on silica gel using eluent gradients to remove short PE-oligomers. Finally, repeated recrystallizations from acetone at -20 °C gradually removed aromatic phosphorous compounds (mainly triphenylphosphine oxide), that possessed identical R_f-values as PPO and were not removed by column chromatography.

Among the pure block copolymers changes of the molecular weight as determined by GPC were too small to reliably calculate degrees of polymerizations for the second block, but ^{1}H-NMR analysis revealed constant PE chain lengths of m = 10 - 12 repeating units for all different PPO block lengths. This is attributed to a similar steric hindrance at all reactive PPO-bound sites, independent of the propylene oxide chain lengths, which differ considerably and probably point to well solubilized blocks openly exposed to the solvent. Thus, the

disappointing PE backbone lengths might be due to intrinsic limitations of the polycondensation approach itself or to some effect during purification that preferentially removed copolymers with longer PE blocks. For comparison reasons, a P*p*PE homopolymer **86** was synthesized directly from the *para*-monomer **85** applying the *in-situ* deprotection protocol (Scheme 6).

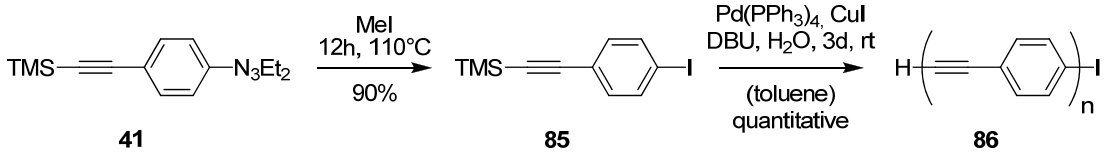

41 **85** **86**

Scheme 6: Activation of unsubstituted para-monomer and its polymerization under Sonogashira conditions using the in-situ-deprotection methodology.

Most of the isolated material was completely insoluble. GPC analysis of the soluble fraction revealed degrees of polymerization of n ≈ 6 - 10. This seams to be the upper chain length limit for unsubstituted soluble poly(*para*-phenylene ethynylene)s.[43-45] The length of the aromatic blocks in the block copolymers compared with the amount of equivalents of monomer used, revealed that around a tenth of all monomers coupled to the PPO. The competing reaction of homocoupling between monomers in solution is much more favorable for reasons of monomer mobility and probability of catalyst encounter as well as of number of reactive sites, i.e. two per monomer and one for the macromolecular capper. The homooligomers in solution then quickly grow to a critical length at which they precipitate and are removed from the reaction mixture before they statistically encounter a block copolymer to couple with.

3.4.2.3 Characterization and Spectroscopy

Figure 7 illustrates the effects of aggregation on GPC traces. On the left side, an activated PPO strand **82b** with a molecular weight of M ≈ 10000 (determined by ^{1}H-NMR) is shown in red. The corresponding block copolymer **84b** still containing P*p*PE-homopolymer impurities is shown in green (the additional low molecular weight signals for the homopolymer are cut off in the representation), the same but purified block copolymer in blue. The bimodal nature of the curve arises from aggregation of the block copolymer. The sharp lower molecular weight signal corresponds to the non-aggregated block copolymer (~32 min. or M_P = 40000) and is only slightly shifted as compared to the parent PPO block **82b** (shown in Figure 7, left, as red trace) because the P*p*PE block contributes only with 1000-1500 mass units to the copolymer. The higher molecular weight signal arises from aggregation of the rod-like segments and the degree of aggregation is noteworthy considering the intensity and retention time of the band. In Figure 7, right, normalized GPC traces of a dilution series of the pure block copolymer **84b** are shown. The band attributed to the copolymer self-aggregation

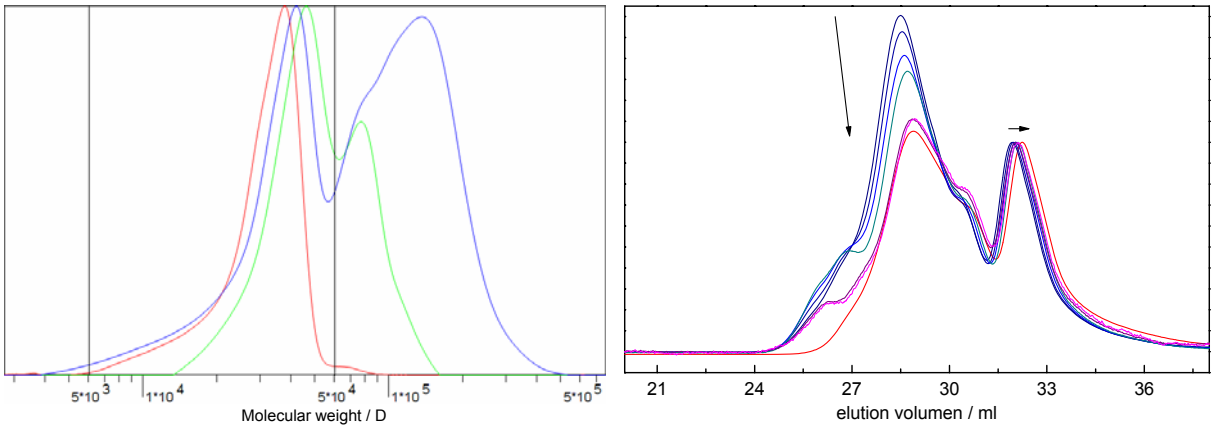

*Figure 7: Overlay of GPC traces: left: activated PPO-block **82b** (red), corresponding PPO-PpPE block copolymer **84b** containing PpPE homopolymer impurities (green), and pure PPO-PpPE block copolymer (blue); right: decreasing and shifting signals upon diluting injection probes of same PPO-PpPE block copolymer **84b**.*

(~28 min.) decreases and shifts to later elution times (i. e. lower molecular weighs) the more diluted the injection samples are, illustrating the dynamic behavior and concentration dependency of the self-aggregation. It should be noted, that in the case of the impure block copolymer (green), the apparently lower degree of aggregation can be explained by the competing P*p*PE homopolymer-block copolymer aggregation, breaking up self-aggregation among the block copolymers.

Bulk characterization by DSC measurement of block copolymer **84b** resembles the data of the corresponding pure PPO **81b**, displaying upon first heating a long shallow endothermic area starting at 28 °C before melting occurs between 57 and 72 °C (Figure 8). Freezing takes place between 38 and 19 °C in a much narrower interval than the pure PPO, indicating the prearrangement of the rod-like segments facilitating crystallization. At the second heating cycle the melting peak at 65 °C is again preceded by a shallow endothermic plateau starting at

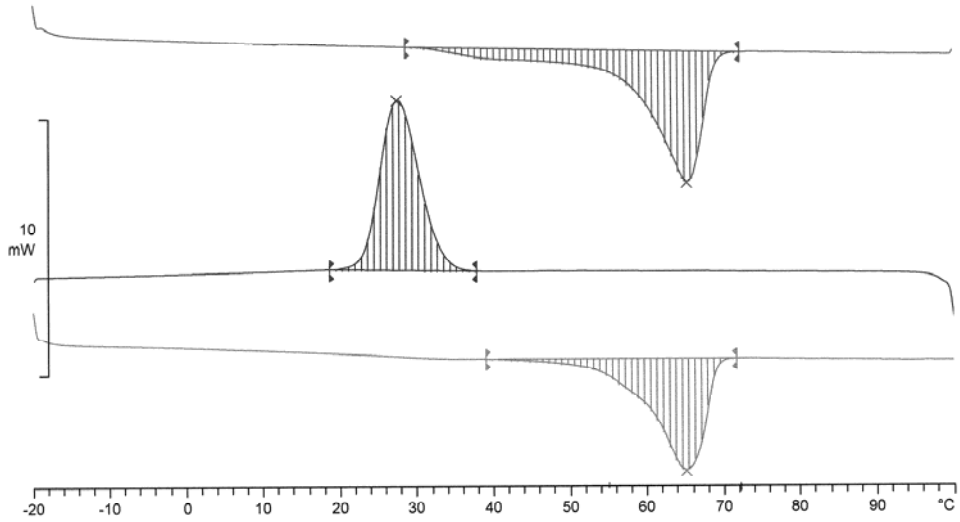

*Figure 18: DSC trace of block copolymer **84b** (Mn = 10000); from top to bottom: first (virgin) heating, cooling, and second heating under nitrogen atmosphere at a speed of 10 K/min.*

39 °C. This reproducible pre-melting might be explained by formation of a liquid crystalline phase among the P*p*PE segment areas.

Initial spectroscopic studies were performed on the block copolymer **84b** with a medium PPO segment length of $M_n \approx 10000$. Absorbance spectra of polymer solutions at same concentrations in different solvents are depicted in Figure 9, left. In chloroform, a more than 50 % increased absorbance was observed, probably due to best solubility and least degree of aggregation of the block copolymer. Here, the absorbance maximum is located at 349 nm. In hexane and methanol, which solvate the aromatic P*p*PE segment less well leading to enhanced aggregation, the absorbance maximum displays a hypsochromic shift to 335 nm, and in

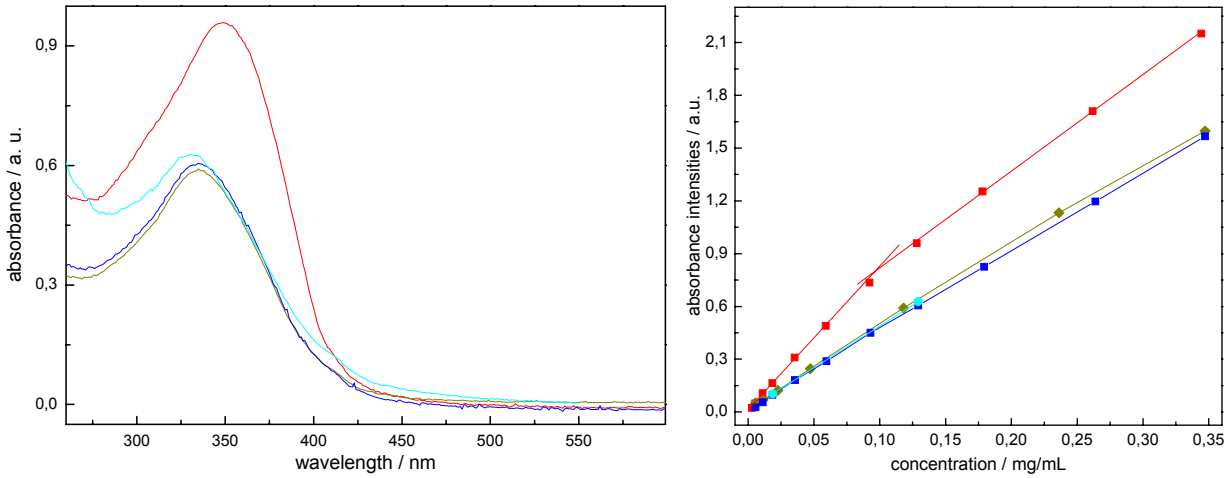

*Figure 9: Left: absorbance spectra of block copolymer **84b** in chloroform (red), hexane (olive), methanol (blue), and methanol-water mixtures (cyan) at identical concentrations; right: absorbance intensities at respective maxima in dependence of concentration.*

methanol-water mixtures the maximum is further shifted to 331 nm. When plotting the absorbance intensities at the respective maxima against concentration, the results in chloroform differ again from those in other solvents (Figure 9, right). In hexane, methanol, and methanol-water mixtures a more or less linear dependency was observed, while in chloroform the slope at low concentrations was much steeper, indicating less aggregation. Increasing the concentration above ca. 0.1 mg/mL initiated aggregation in $CHCl_3$, too, and absorbance increased slower at a rate similar to the ones of other solvents.

Large differences were observed in the fluorescence spectra. The emission curves of **84b** in several solvents are shown in Figure 10, left. All signals are essentially bimodal possessing a peak at lower wavelengths corresponding to non-aggregated P*p*PEs and a peak at longer wavelengths caused by excimer emission[1] of aggregated and interacting aromatic units. In chloroform, which solvates both block segments of the copolymer, the hypsochromic signal is

[1] More correctly, a pseudo-excimer effect is observed, as the interacting aromatic moieties are pre-organized face-to-face due to aggregation.

much stronger confirming the relative good solubility of the copolymer. In methanol, both peaks have similar intensities (see Figure 10, right) and the overall emission intensity is dramatically reduced due to strong fluorescence quenching, and in methanol-water mixtures hardly any fluorescence was detectable, inhibited by strongest tendencies towards aggregation (no reliable ratio determination possible). Remarkably is the emission in hexane. The shape of the bimodal emission curve resembles the curve in chloroform in terms of peak ratio and overall intensity, but the curve is hypsochromatically shifted by 13 to 16 nm. The peak ratios develop upon concentration changes nearly identical to the changes observed in chloroform (Figure 10, right). In chloroform, both blocks of the copolymer are well soluble, limiting

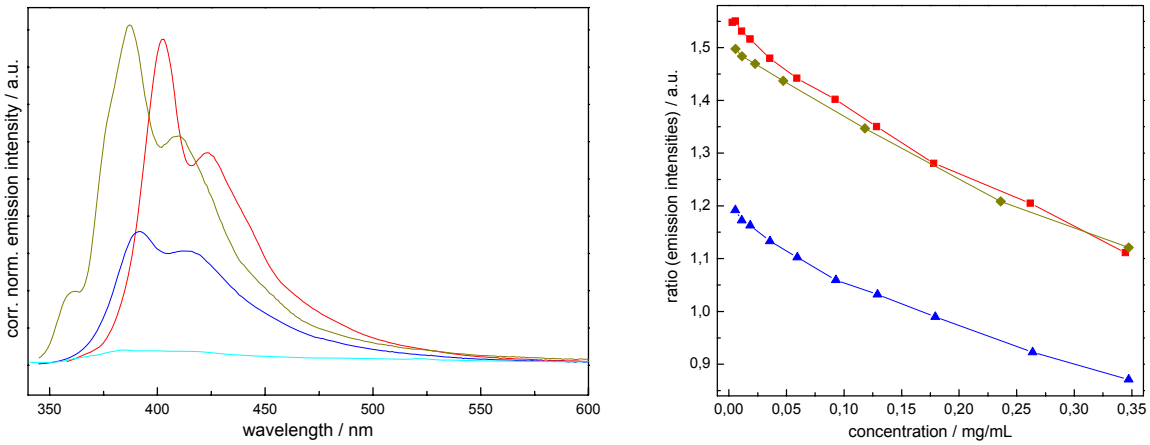

*Figure 10: Left: emission spectra of block copolymer **84b** in chloroform (red), hexane (olive), methanol (blue), and methanol-water mixtures (cyan) at identical concentrations; right: ratio of emission intensities in dependence of concentration.*

aggregation and explaining the lack of optical activity (Figure 11). But in contrast to chloroform, optical activity is present in hexane solutions and resembles the activity in methanol. As methanol solvates PPO but not P*p*PE, the block copolymer aggregates with the rigid block presumably assembling into chiral stacks with the PPO segments showing outwards into the solvent and forming the sheath around the stacks keeping the supramolecular structure in solution. As the stacking occurs with a preferred twist sense induced via chirality transfer from the PPOs, an optical activity is observed. Increasing the effect of amphiphilicity in the copolymer by adding water as co-solvent does further quench fluorescence, but in terms of optical activity a saturation was already achieved in pure methanol. Hexane resembles a poor solvent for both PPO and P*p*PE segments and the PPO strand adopts a more compact coil structure presumably embedding the rod-like aromatic block. This leads to, first, a polarity change around the P*p*PE and explains the hypsochromic shift in absorbance, second, isolates the aromatic blocks from each other giving raise to strong non-aggregating signals in the fluorescence, and third, generates a chiral environment around the aromatic backbone explaining the optical activity in absence of aggregation.

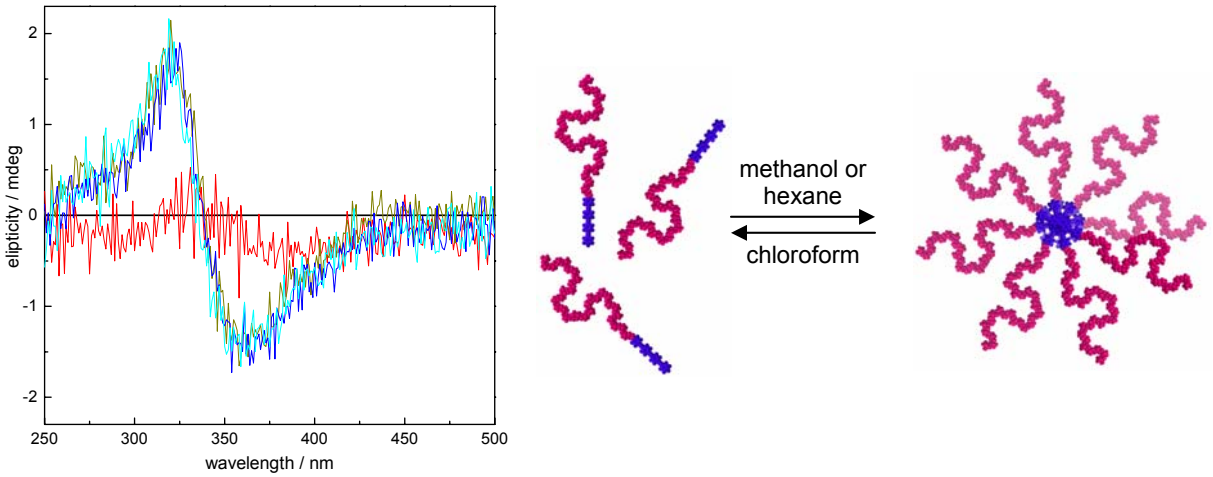

*Figure 11: Left: CD spectra of block copolymer **84b** in different solvents normalized to same optical density; — chloroform, — hexane, — methanol, — methanol:water = 2:1; right: cartoon illustrating ordered assembly into chiral stacks in polar solvents.*

In general, temperature plays a role in aggregation phenomena, i. e. heat breaks up assemblies and increases solubility of individual components. This effect is also observed among block copolymers as shown in Figure 12. While the effect on absorbance is minor (not shown), fluorescence is increased upon heating block copolymer **84b** from 10 to 50 °C in methanol due to reduced aggregation. The effect is stronger in methanol than in chloroform (Figure 12, right), as in the latter solvent both blocks are well soluble.

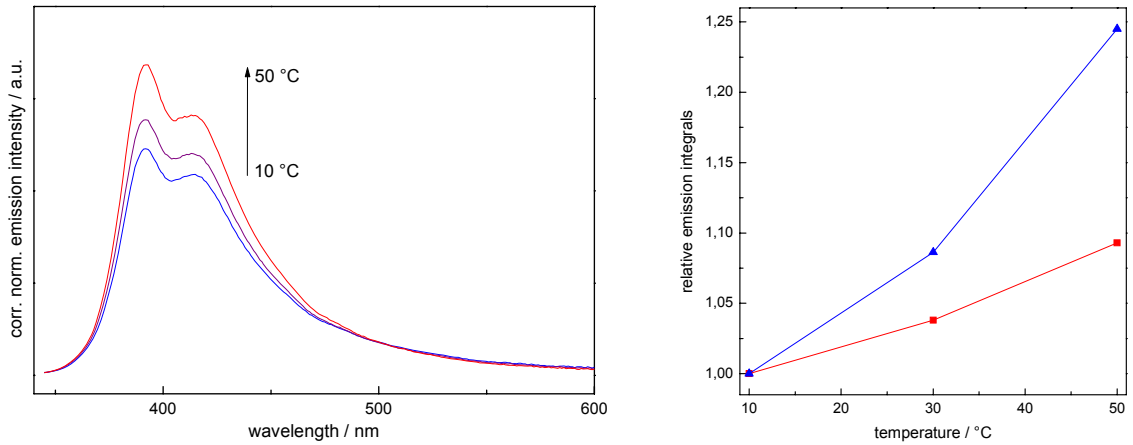

*Figure 12: Temperature effect on fluorescence spectra of block copolymer **84b**: emission spectra in methanol (left) with an OD ≈ 0.1, and integral values of emission spectra at different temperatures (right) in chloroform (■) and methnol (▲).*

The behavior of the other block copolymers with shorter and longer PPO segments, **84a** and **84c**, respectively, is similar for the different solvents. For **84c**, absorbance maxima shifted to lower wavelengths with increasing solvent polarities (Figure 13, left). The bimodal fluorescence spectra display the same features of low aggregation in chloroform, similar peak ratio and quenching in methanol and strongest quenching in methanol-water mixtures (Figure 13, right). Here, fluorescence is not totally quenched due to the superior solubilizing power of the longer PPO segment compared to copolymer **84b**.

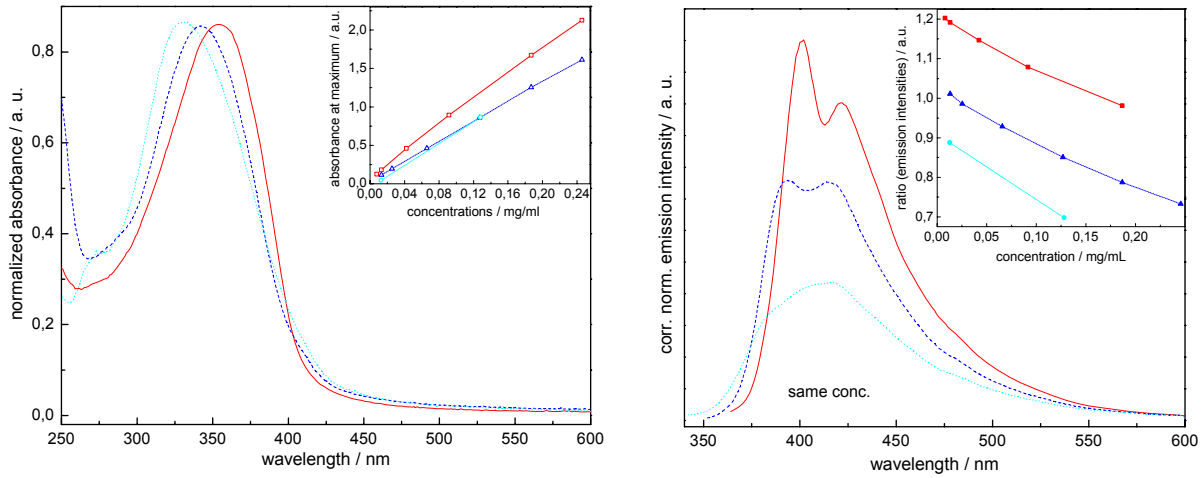

*Figure 13: Absorbance (left) and emission (right) spectra of block copolymer **84c** in chloroform (solid red), methanol (dashed blue), and methanol:water mixture (dotted cyan) at same concentrations; fluorescence spectra at same optical density of ~ 0.1. Insets illustrate absorbance maxima intensities (left) and emission peak ratio (right) against concentrations for different solvents.*

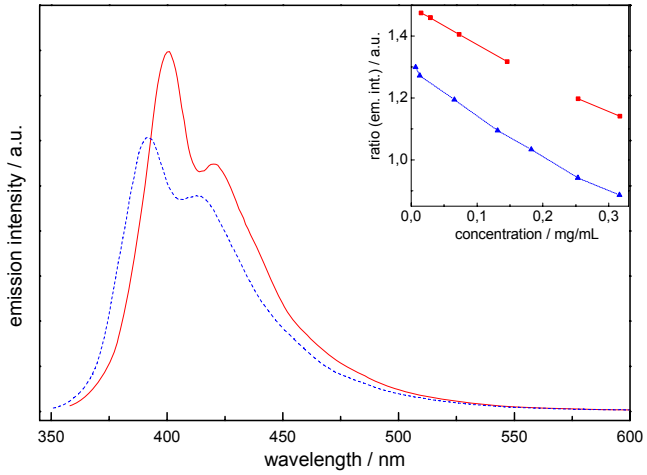

*Figure 14: Emission spectra of block copolymer **84a** in chloroform (solid red) and methanol (dashed blue) at same concentrations and optical densities of ~ 0.1.*

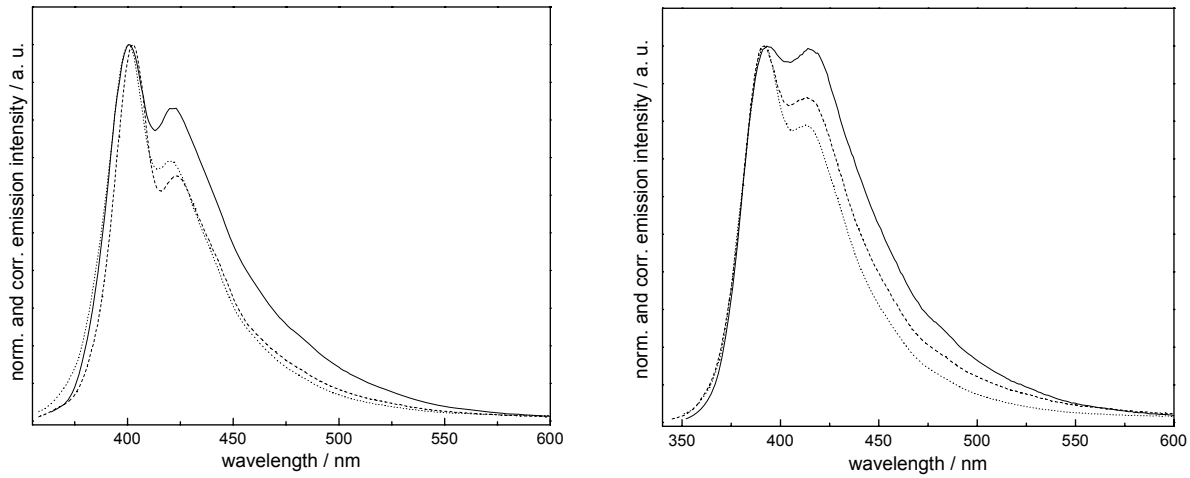

*Figure 15: Fluorescence spectra of block copolymers **84a-c** in chloroform (left) and methanol (right). **84a** (dotted), **84b** (dashed), **84c** (solid). Spectra normalized to same intensities.*

Also block copolymer **84a** shows similar behavior to the other copolymers. In methanol, the absorbance maxima is shifted to lower wavelengths (not shown) and the fluorescence is blue-shifted and partly quenched and the peak ratio changed in favor of the longer wavelength signal (Figure 14). Overlays of absorption spectra in chloroform and methanol for all three block copolymers **84a-c** are shown in Figure 15 to study the influence of the PPO block length on the aggregation. All spectra were normalized to same intensity for better comparisons. In chloroform the emission spectra for **84a** and **84b** look more or less the same, while the spectrum for **84c** with the longest PO segment possesses features indicating an increased presence of excimers. In methanol, the shorter the PPO chain length the less intense develops the signal at longer wavelengths attributed to excimer emission. Apparently the long

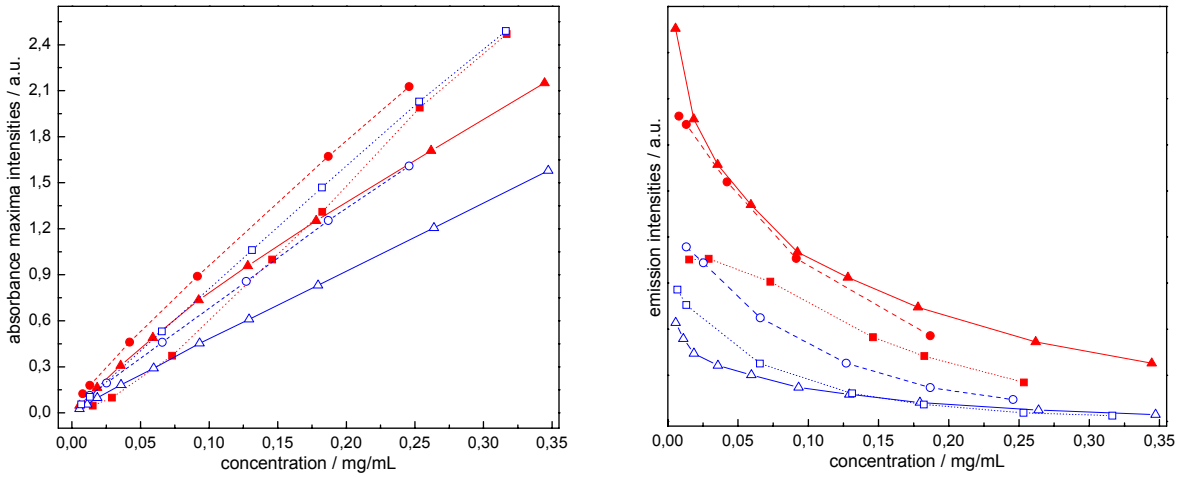

*Figure 16: Absorbance maxima intensities (left) and emission intensities (right) against concentration for different block copolymers **84a-c** in chloroform (red, opaque symbols) and methanol (blue, hollow symbols); ■ **84a**, ▲ **84b**, ● **84c**.*

PPO segments of **84c** better support the existence of aggregates due to superior solubility and better shielding of the assemblies. Figure 16 illustrates the changes of absorbance and emission against concentration for all three copolymers in different solvents. The summary of the absorbance data (left) does not reveal unequivocal conclusions. In principle, absorbance raises faster in chloroform than in methanol due to less pronounced aggregation while concentrating sample solutions. Likewise, copolymers display stronger emission in chloroform than in methanol (right). The fluorescence data show that in chloroform the copolymer **84a** with the shortest PPO segment possesses the least intense emission of all copolymers (although still more intense than any copolymer in methanol), and consequently, in methanol the copolymer **84c** with the longest PPO block displays less quenching than the other copolymers with shorter PPO segments.

In Figure 17, CD spectra of block copolymers of the type PPO-*b*-P*p*PE are shown. In chloroform (left), both block segments of the series **84a-c** are well solubilized. Thus no

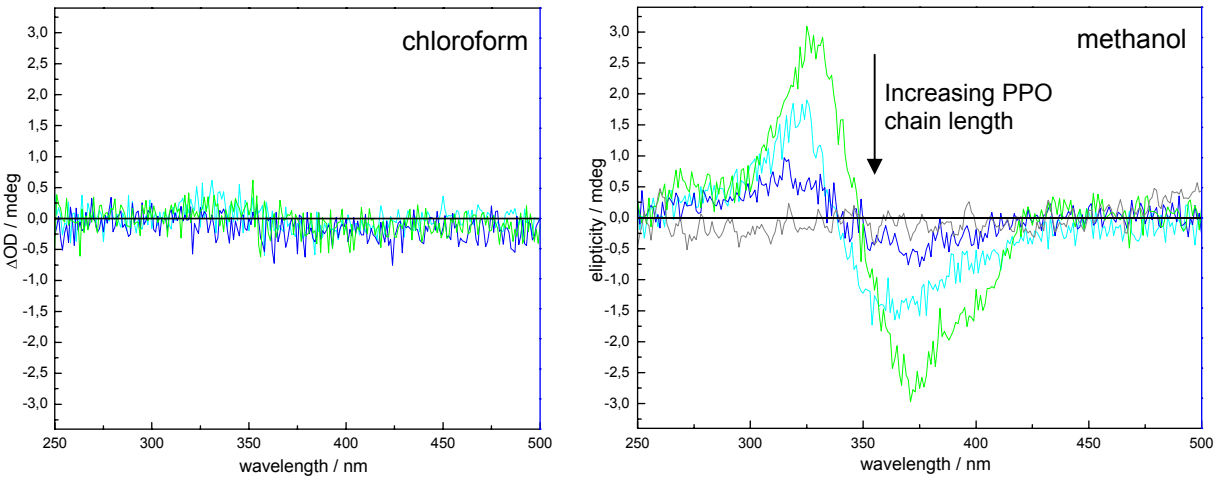

*Figure 17: CD spectra of block copolymers **84a-c** in chloroform (left) and methanol (right) at same concentration and normalized optical densities of OD = 1; — **84a**, — **84b**, — **84c**.CD spectrum of atactic PPO-based block copolymer **97**(—) in methanol included in right figure.*

aggregation occurs and no chirality transfer takes place. Instead, in methanol the aromatic segments aggregate to presumably chiral stacks with a preferred screw sense thus giving rise to a CD signal between 300 to 425 nm (figure 17, right). The tendency to aggregate depends primarily on two factors, the solubilizing power and the bulkiness of the PPO block. The excellent solubilizing power of the longest PPO block in **84c** accounts for a still good solubility of the whole block copolymer in methanol and at the same time complicates stacking of the aromatic segment due to his bulkiness leading to either shorter or less ordered stacks. Thus, the optical activity is the lowest among the three block copolymers of differing PPO chain lengths. On the other extreme, block copolymer **84a** with the shortest PPO strand displays the strongest optical activity for the same reasons given before, i. e. lower solubilizing power due to reduced PPO chain length and smallest bulkiness to thwart stacking propensity. The compilation on the right displays in addition the CD spectrum for block copolymer **97**, an analogue of **84b** possessing an atactic PPO block. Both block copolymers generate similar absorbance and emission spectra, but concerning optical activity, no CD signal is observable in methanol, as no chiral information can be transferred to the aromatic P*p*PE block. The absolute values for optical activity are moderate due to a nearly parallel stacking of the rod-like P*p*PEs allowing for the best aromatic π-π-overlapping. The ideal stacking distance of planar aromatic systems is 3.5 Å, whereas PPO strands adopt a distance of at least 4.7 Å in the crystalline bulk as determined by X-ray analysis.[18, 51] This incompatibility leads to a less ordered organization and thus to a low transfer of chirality.

3.4.3 Poly(*meta*-Phenylene Ethynylene)s in Block Copolymers

3.4.3.1 Introduction

The incorporation of a reversibly foldable segment into a block copolymer should enable dynamic changes in the aspect ratio of the copolymer as the foldamer segment switches between compact helical and rod-like conformations (Figure 19, center). Major factors influencing supramolecular assembly constitute amphiphilicity as well as shape of the building blocks.[52] As illustrated in Figure 19, switching of the aspect ratio may lead to different ordered structures such as lamellar packing of extended linear block copolymers or curved micelle formation from wedge-shaped macromolecules. The mere combination of a "switchable" segment and a "functional" segment should therefore allow for the versatile, fast, and convenient generation of custom-tailored hybrid materials. *meta*-Connected phenylene ethynylene backbones are predestinated for the switching segment as they dramatically alter spatial dimensions upon folding due to low pitch and fair number of repeating units per turn. In a block copolymer, the non-PE block could provide solubility and amphiphilicity, thus allowing the use of unsubstituted phenylene ethynylene monomers and simplifying chemical structure and synthesis.

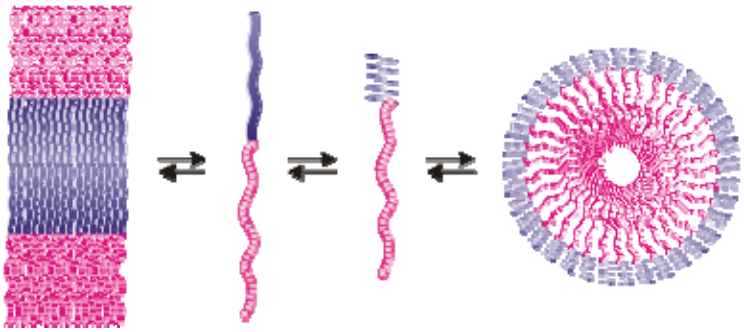

Figure 19: Conformational changes from rod-like to helical shapes of one block (blue) on a block copolymer alters overall aspect ratio (center) and potentially lead to different aggregation modes like lamellar (left) or spherical (right) supramolecular arrays.

Trumbo and Marvel reported on unsubstituted soluble P*m*PEs of a maximum length of 15 repeating units and on completely insoluble P(*m*-alt-*p*-PEs).[53] The lack of solubilizing side chains and the structure's rigidity and flatness promote aggregation. Although random kinks in the backbone in general weaken chain-chain interactions and delay aggregation, here, the high structural regularity in the all-*meta*-PE-backbone again eases intermolecular contact and aggregation of, e. g. the planar and flat zigzag conformation. The closest structure resembling unsubstituted PmPEs so far, is Anderson's bis-silyl terminated PE-pentamer with three *meta*-kinks in the backbone.[49]

3.4.3.2 Synthesis of unsubstituted Poly(meta-Phenylene Ethynylene) Homopolymers and Block Copolymers

The synthesis of the monomer proceeded with ease in four steps. The amino group of 3-iodoaniline **87** was masked as a triazene via a diazonium intermediate. Coupling of an excess of TMS acetylene (TMSA) with the aryl iodide **88** gave the bisprotected *meta*-monomer **89**. The yield was surprisingly low compared to similar couplings involving TMSA and simple aryl iodides. Transformation of the triazene moiety under standard conditions to the corresponding iodo compound proceeded smoothly. However, during up-scale of this transformation an explosion of the reaction vessel was encountered. An alternative synthetic route – shorter but involving a more challenging separation – gave **77** directly upon monocoupling of TMSA onto *meta*-diiodobenzene (Scheme 7, bottom). Desilylation of the acetylene under basic conditions or by fluorides provided the desired monomer **78** with two orthogonal functionalities for Sonogashira couplings in quantitative yields.

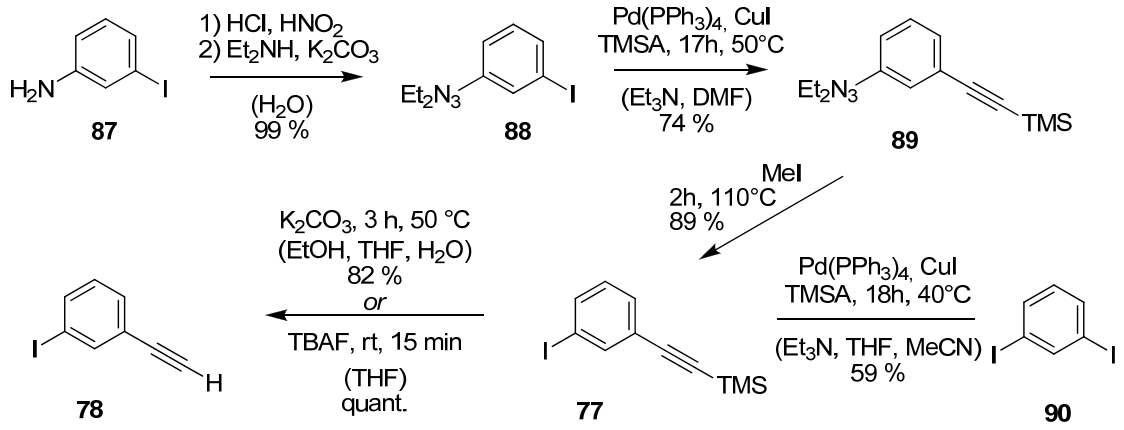

*Scheme 7: Linear 4-step synthetic route to meta-ethynyl-iodobenzene monomer **78** starting from meta-iodoaniline (top) and shorter route based on meta-diiodobenzene (bottom).*

The synthetic procedure to PPO-*b*-P*m*PE block copolymers resembles the one for PPO-*b*-P*p*PE block copolymers. The same PPO derivatives **82** – activated by esterification with iodobenzoic acid – were each mixed with an 100-fold molar excess of *meta*-monomer **78** and submitted to Sonogashira polycondensation reactions (Scheme 8). The crude block copolymers were easily generated, but again purification was tedious, as the concurrently produced homopolymer P*m*PE formed stable colloidal complexes with the block copolymer and phosphorous compounds always co-precipitated with the block copolymer during the last purification steps. These obstructions dramatically lowered the yields as much material was lost along several purification steps. Again, highly pure material was needed to determine the length of the aromatic block by ^{1}H-NMR, as GPC differences were too small to be reliable and calibration with polystyrene samples lead to erroneous values in this case. Independent of

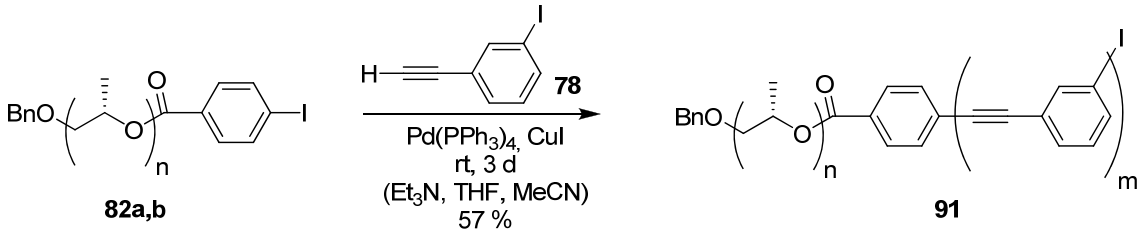

Scheme 8: Generation of rod-coil block copolymers by polycondensation of meta-ethynyl-iodobenzene to suitable PPO blocks (a: n ≈ 100, M_n = 5000, b: n ≈ 200, M_n = 10000; m = 8 - 10).

the length of the PPO block, polymerization degrees for the PmPE block were always around m = 8 - 10 repeating units, hence on the verge of being able to fold into stable helices. According to Moore, an amphiphilic electron-poor *meta*-phenylene ethynylene backbone starts to fold at a length of 10 to 12 repeating units and a corresponding less electron-deficient backbone would need more repeating units to adopt a stable helix, [54] as stabilization by aromatic π- π-interactions weaken with increasing electron density in the aromatic rings.[55] Nevertheless, optical spectroscopy experiments were recorded and the results are presented in the next section.

In order to increase the length of the rod-segment, an alternating approach to block copolymers – the condensation of two pre-formed PPO and P*m*PE blocks – was targeted. *meta*-Connected monomer **78** was polymerized to the corresponding unsubstituted P*m*PEs **92** under various reaction conditions to obtain polymer chains as long as possible with high monomer conversions and at the same time minimize formation of insoluble high molecular weight polymers that lower the yield of further utilizable material (Scheme 9).

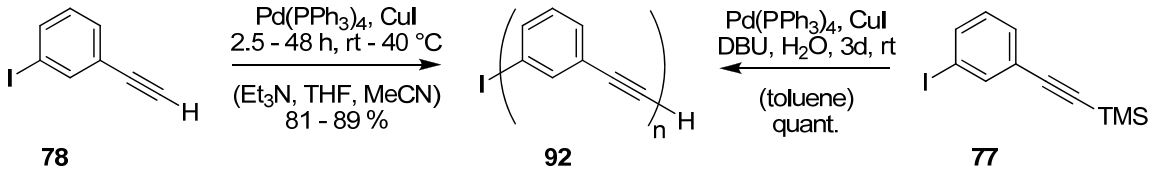

Scheme 9: Polymerization of meta-ethynyl-iodobenzene under varying conditions to optimize chain length and yield of soluble polymer fraction.

Variations of reaction time as well as temperature, catalysts loading, and moderate concentration changes culminated in a maximal molecular weight of soluble P*m*PE of M_n = 4500 and a Gaussian weight distribution after 20 h, as determined by GPC. Longer reaction times of up to two days and higher temperatures to delay polymer precipitation did not visibly increase molecular weight or change the shape of the GPC trace. The polymerization of the corresponding TMS-protected monomer **77** – applying the *in-situ*-desilylation protocol – rendered basically the same insoluble P*m*PE with similar molecular weights for the soluble fraction.

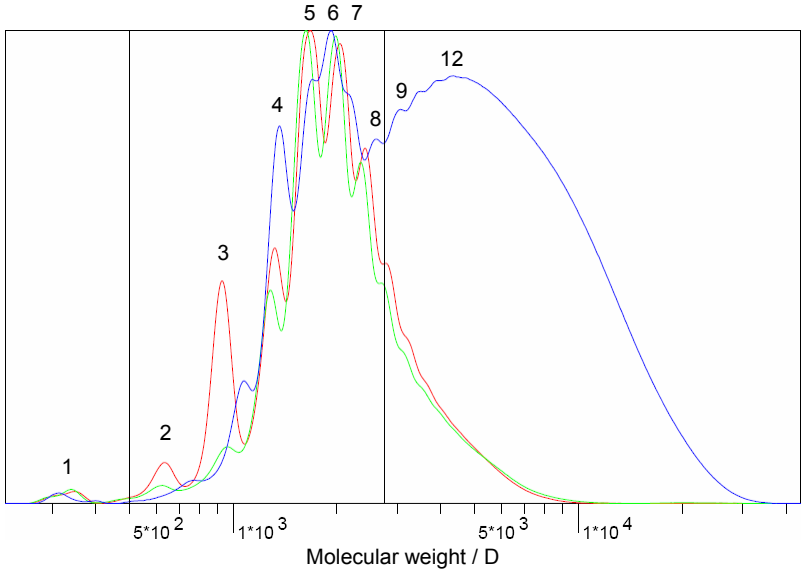

Figure 20: Overlay of GPC traces (280nm UV detector) from PmPE samples taken out of polymerization mixture after 2.5 h (red), 6.5 h (green), and 20 h (blue). Labels indicate number of r. u.

At first sight all the obtained molecular weights are respectable with values of Mn = 4500 corresponding to 45 repeating units (100 g/mol per r. u.), but the GPC-determined maximum molecular weights are highly overestimated, as PPEs possess a much larger rigidity than polystyrene that is used to calibrate the GPC system. The hydrodynamic volume adopted by a repeating unit is comparable to the monomer itself and is set to ~ 300 as calculated from the GPC trace of the monomer. This value translates to an approximate average number of repeating units of only n = 15. Figure 20 shows the overlaid GPC traces of PmPEs polymerized between a few and 20 hours. Monomer at M_n = 300 was quickly consumed and barely detectable already after 2.5 hours. The two traces for the early samples hardly differ from each other, with the very first sample just displaying higher intensities for oligomers up to the tetramer. Instead, the latest sample shows the typical Gaussian weight distribution but still with outstanding lower oligomer signals on the low molecular weight slope. Reprecipitations in different solvents removed these shorter oligomers and slightly shifted the curve to higher molecular weights and improved its shape, but at the expense of high mass losses. Starting with the signal for the monomer and counting the individual signals on the low molecular weight slope of the GPC curve corresponding to oligomers of increasing length, lowers the degree of polymerization to n ≈ 12 at the curve's maximum.

In consideration of these results, no practical benefit from the coupling of these pre-formed P*m*PE blocks with a PPO segment would be gained as compared to the first approach of directly polymerizing an *m*PE monomer to the PPO and thus, this route was not followed further.

3.4.3.3 Characterization and Spectroscopy

The effects of different solvents and concentrations on the potential folding reaction were determined by monitoring UV absorbances as well as absorbance ratios that have been identified to correspond to both the folded and random coil states.[56] The absorbance spectra of block copolymer **91b** consist of one band with two pronounced peaks (Figure 21, left). The ratio of these peaks versus the concentration are plotted in the same figure, right. Methanol, which is a poor solvent for the aromatic segment and thus should promote folding, indeed gives lower absorbance ratio values compared to chloroform as described in literature, consistent with an increasing population of the (partially) folded conformation. Upon concentration these ratio values increase for both solvents and converge, hence indicating "unfolding". This unusual behavior might be explained by a starting lamellar aggregation in solution where aromatic segments adopt an extended planar zigzag conformation for better packing, thus explaining the additional "unfolding" of P*m*PE in chloroform, i. e. with increasing concentration, aggregation is facilitated and helical (more pronounced in methanol) or random coil (in chloroform) conformations change into the extended conformation resembling the preferred assembly mode, similar to Moore's solid state arrangement modes of O*m*PEs.[57]

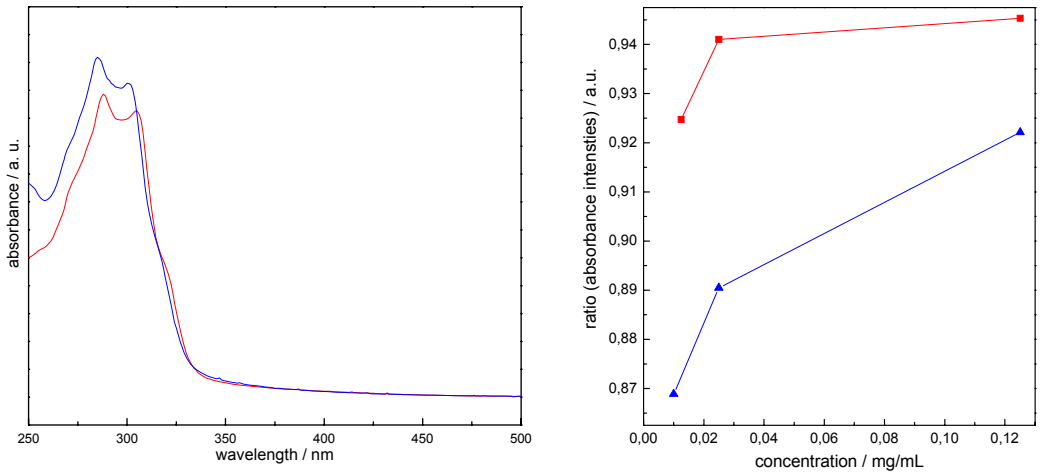

*Figure 1: Left: absorbance spectra (left) of PPO-b-PmPE block copolymer **91b** in chloroform (red) and methanol (blue; right: corresponding absorbance ratios in dependence of concentration and solvent: ■ 305/288 in chloroform, ▲ 301/285.*

The emission in chloroform resembles a narrow intense monomodal signal with little off-tailing, typical for unfolded and non-aggregated *meta*-phenylene ethynylenes (Figure 22, left). In contrast, the emission in methanol is partly quenched due to aromatic interactions and at the same time, the broad band of π-π-excimer emission is observable as a second feature above 400 nm indicating partial folding.

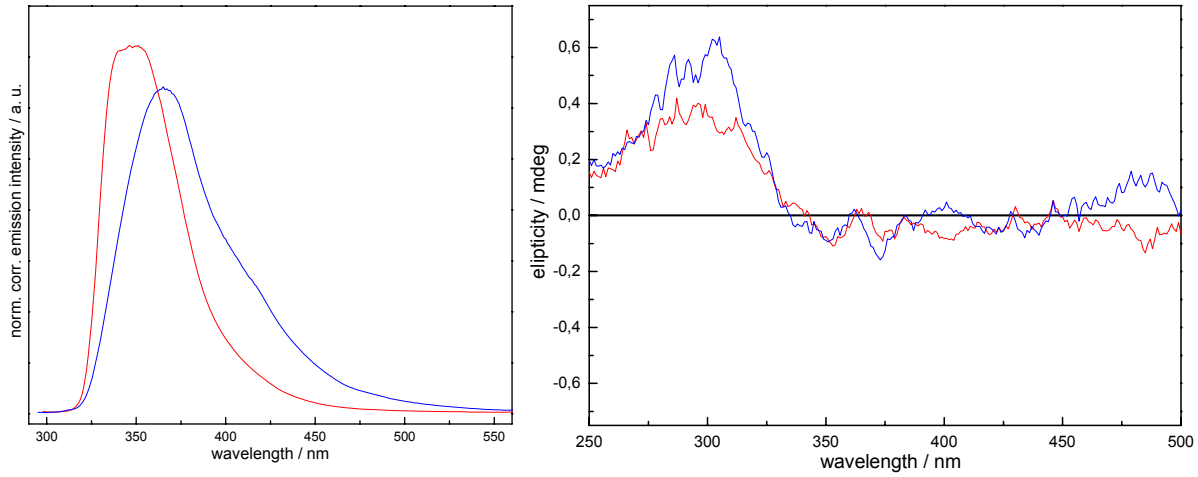

*Figure 22: Emission (left) and CD (right) spectra of block copolymer **91b** in chloroform (red) and methanol (blue) at same concentrations. Excitations at the lower absorbance maxima of 285 nm and 288 nm, respectively, with an optical density of 0.1. CD spectra recorded with an optical density of 1.*

Solvent effects on the CD signal are small. In methanol as well as in chloroform a positive signal in the region of PE backbone absorption is observed (Figure 22, right). Chirality transfer also occurs in the unfolded conformation in chloroform, probably due to certain lamellar aggregation (*vide supra*). As the P*m*PE backbones are very short, no large signal changes are expected, if at all; nevertheless, an increase in elipticity in methanol is observed. The fraction of longest backbones in the polydisperse P*m*PE segment might fold and give rise to the observed effect. In addition, folding might be strengthened by a total wrapping of the aromatic backbone by the much larger PPO strand, thus encapsulating and stabilizing whichever labile PE conformation has been adopted.

The DSC measurement resembles the data of pure PPO, displaying upon first heating a long shallow endothermic area starting at 30 °C before melting occurs between 54 and 74 °C. Freezing takes place between 44 and 20 °C, while during the second heating cycle the melting peak at 68 °C is preceded by an exothermic rearrangement.

3.5 Graft Copolymers

3.5.1 Introduction

Only few examples exist of PPE-based graft copolymers. Swager and coworkers[58] synthesized a P*p*PE carrying radical initiators and subsequently polymerized styrene side chains onto it, thus generating a graft copolymer displaying polarized photoluminescence in film blends (Figure 23, left). Perahia and Bunz reported on a grafted copolymer based on a poly(*para*-phenylene ethynylene) backbone and polyester side chains[59] by, first, polymerizing caprolactone on an aromatic building block and, second, homopolymerizing the

aromatic building blocks (Figure 23, right). Two different non-reversible morphologies in films were observed; i.e., spherical entities of solvent-induced kinetically trapped aggregates dominated by the side chains, and after annealing a needle-like phase arising from the now dominating main chain aggregation.

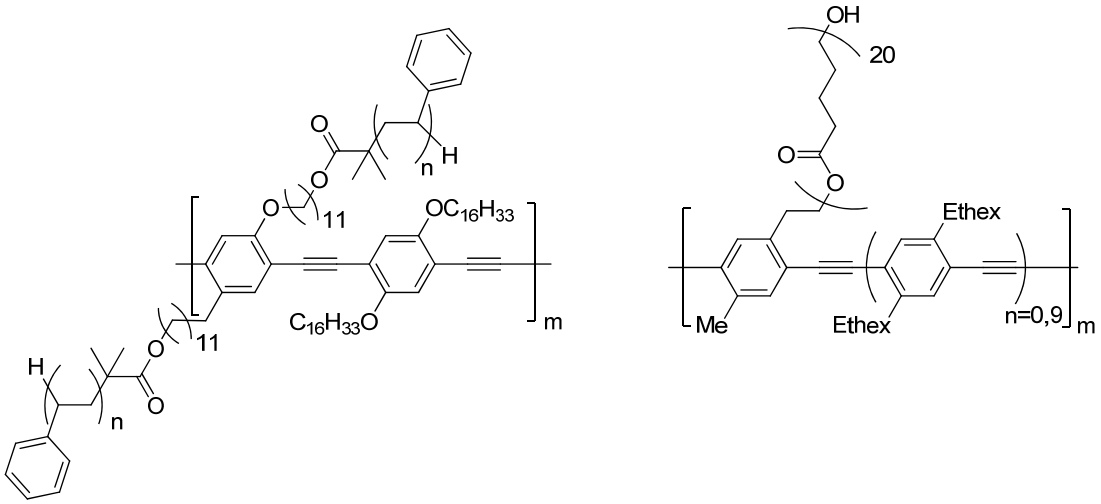

Figure 23: Reported graft copolymers based on poly(para-phenylene ethynylene)s.

Our approach targets on morphology changes that are, first, based on a conformational change of the backbone, and second, are reversible and can thus be switched by external stimuli. To achieve this goal, a *meta*-connected P*m*PE backbone is used, capable of undergoing well-known solvophobically driven helix-coil transitions, and grafted to it, a PPO side chain to introduce the required amphiphilicity and enlarge the overall object size (Figure 24). This should lead to a large change in aspect ratio in the event of folding and show the potential to access smart responsive materials. The monitoring of folding among *m*PEs is well established and includes optical spectroscopic techniques like absorption and fluorescence spectroscopy. The utilized PPO block will be based on the enantiopure (*S*)-propylene oxide monomer, thus CD spectroscopy can be additionally used to verify chirality transfer and folding.

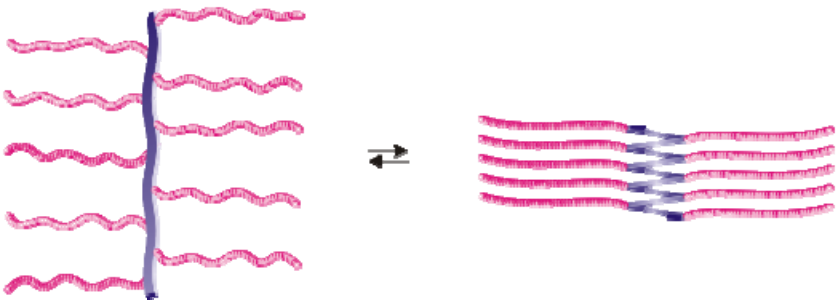

Figure 24: Large change of aspect ratio upon backbone folding of a poly(m-phenylene ethynylene)-graft-poly(propylene oxide) brush.

3.5.2 Synthesis

The synthesis followed a linear route based on the trifunctional monomer 3-(TMS-ethynyl)-5-iodobenzoic acid **93**[60] (Scheme 10). This monomer carried again two orthogonal functional groups for the final Sonogashira polycondensation. First, esterification of the benzoic acid with a hydroxyl-terminated poly(propylene oxide) **81** at room temperature using DIC and DPTS reagents gave the TMS-protected macromonomer **94**. DPTS represents the equimolar adduct of DMAP and *para*-toluenesulfonic acid; while the pyridine derivative and carbodiimide activate the benzoic acid and thus allow for esterification using carboxylic acids, toluenesulfonic acid is reported to suppress the side reaction to N-acylureas.[61] Initial esterification attempts with HOBT and EDC, standard reagents for amino acid couplings, failed to achieve complete coupling. In all esterification reactions, an excess of the benzoic acid component was used to ensure complete coupling of the difficult to access PPO terminus, as unreacted PPO would have been impossible to separate from the product. The often problematic urea side product was completely removed together with the excess of monomer by repeated precipitations in toluene, where the macromonomer showed good solubility.

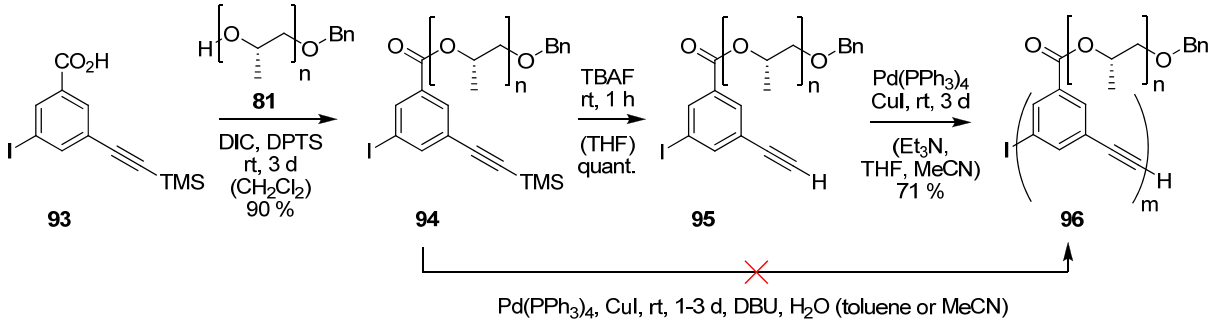

Scheme 10: Folding graft copolymers: synthesis of PPO-esterified macromonomer and its Sonogashira polycondensation.

Direct Sonogashira polycondensation of macromonomer **94** applying the *in-situ* acetylene deprotection protocol was unsatisfactory. As this polymerization includes the usage of base and water, partial saponification of the benzoate was observed by GPC in all attempts and could not be prevented by optimizing reaction conditions. Thus, the silyl group was removed in an extra reaction step with TBAF, allowing the reaction to procede for a relative long time of one hour to ensure full deprotection of the embedded reactive site. Now, polycondensation of **95** under standard and water-free conditions gave the desired graft copolymer **96** with no detectable saponification. The GPC trace of this copolymer together with the corresponding macromonomer is shown in Figure 25, left. On the right side, the absolute molecular weight was determined via a GPC-viscosity-coupling methodology as M_n = 110000 and M_w = 201000, respectively. The absolute molecular weight of the macromonomer was determined

by ^{1}H-NMR endgroup analysis. Thus, the degree of polymerization could be reliably calculated as n ≈ 11 with an polydispersity of n = 5 to 50, and enabling potential folding into helical conformations. Independently, determination of molecular weight by ultracentrifugation gave values for M_W = 240000 in agreement with previous absolute weight determinations.

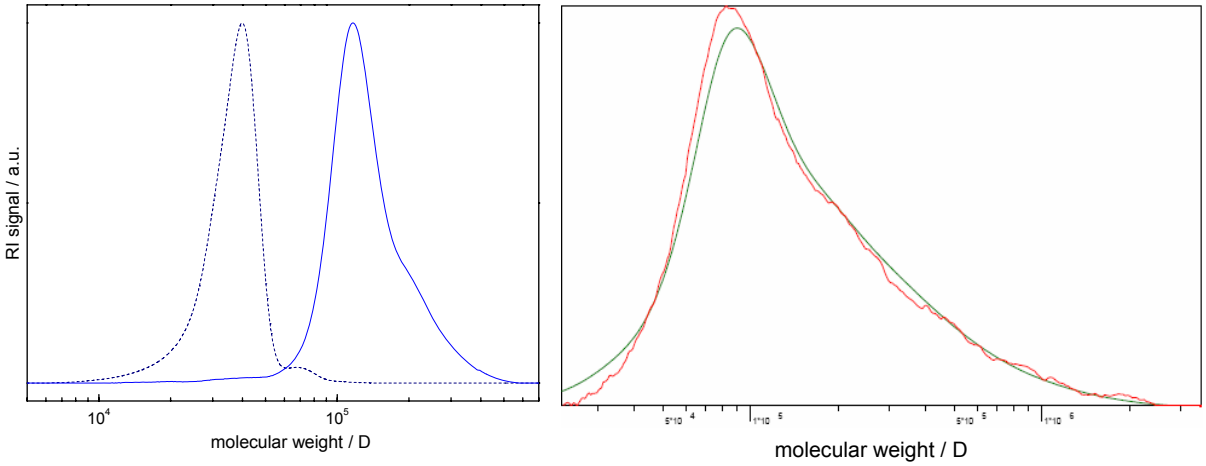

*Figure 25: Overlay of GPC traces of macromonomer **95** (dashed line) and corresponding graft copolymer **96** (solid line) against polystyrene standard (left), GPC trace of same graft copolymer calibrated with viscosimeter showing absolute molecular weights (right).*

3.5.3 Spectroscopy

The results from optical spectroscopy are shown in Figure 26. The absorbance spectra in different solvents are very similar, possessing the same features in comparable intensities. Among *meta*-phenylene ethynylenes, folding is monitored by a decrease of the shoulder at 300 nm when going from chloroform to more polar solvents like acetonitrile or methanol. This was only observed after adding water as a co-solvent. Similarly, the fluorescence curves differ in shape around their maxima, but possess comparable intensities. Why the emission in acetonitrile or methanol was stronger than in chloroform remains unclear. Again, only upon water addition a decent quenching and broadening was observed together with the arising of a new shoulder above 400 nm attributed to excimer formation among adjacent aromatic backbones. An overlay of CD spectra is shown in Figure 27 illustrating the solvent-driven induction of optical activity. In chloroform a minor activity is observed, as the aromatic backbone probably adopts an extended conformation in order to minimize steric repulsion of the bulky PPO side chains. In polar solvents like acetonitrile or methanol, an increase of optical activity is observed, attributed to the helical folding of the backbone, which retreats from the solvent. The moderate effect might be explained by either an inefficient chirality

transfer from the PPO chains to the aromatic backbone or by a hindered folding. To attain a stable helix with favorable aromatic π-π-interactions between turns, a pitch of 3.4 Å has to be achieved, while crystalline PPO strands pack in the bulk with distances of 4.7 Å, thus conflicting with the folding event.The PPO chains with a mass of M_n = 10000 g/mol (DP = 200) are very long and numerous compared to the dimensions of a helical turn thus contributing substantial bulkiness to the system. While a helical backbone possesses an outer diameter of 17 Å, the extended PPO chains spread across over 700 Å. As PPO chains are condensed to every repeating unit of the backbone, much steric constrains might be generated and limit the conformational freedom and tendency to fold of the P*m*PE backbone. Stacking of short helices would further stabilize this conformation, but is again aggravated by the bulkiness of PPO side chains wrapping up the aromatic backbone.

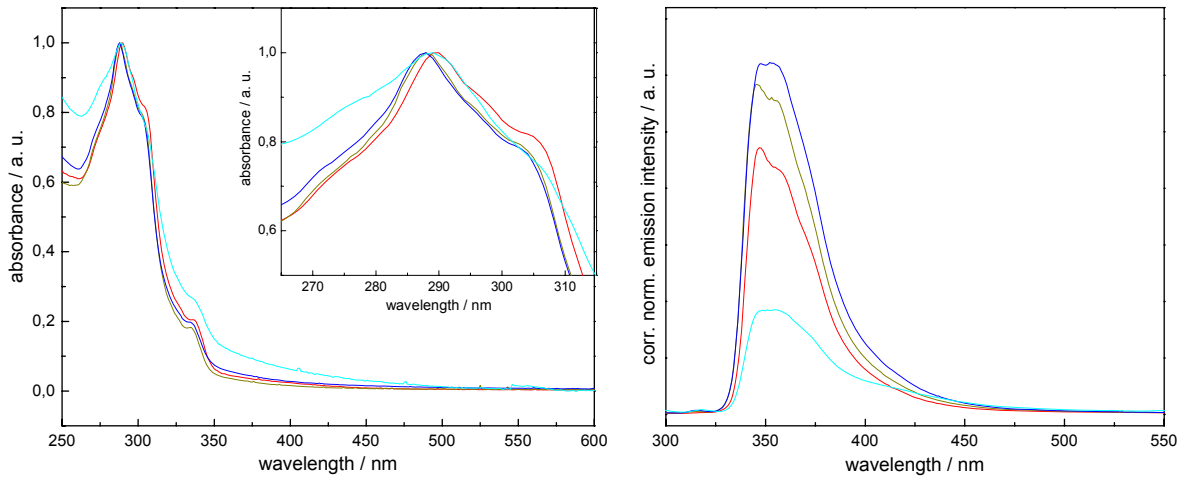

*Figure 26: Absorbance (left) and emission (right) spectra of graft copolymer **MB256** in chloroform (red), acetonitrile (olive), methanol (blue), and methanol-water mixture (cyan). Inset shows a magnification of the peak area.*

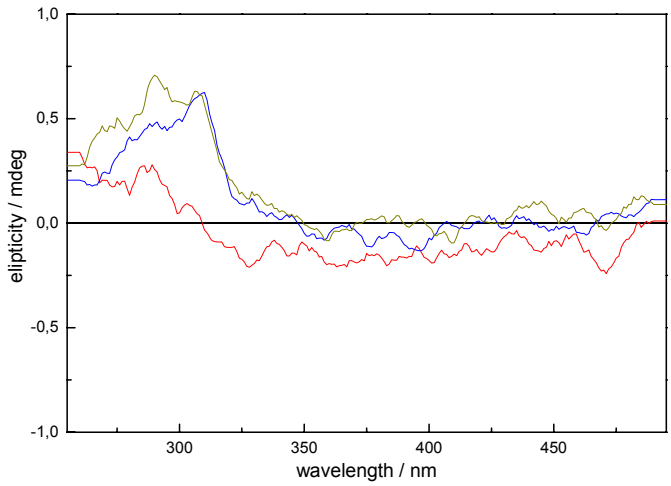

*Figure 27: CD spectra of graft copolymer **MB256** in chloroform (red), acetonitrile (olive), and methanol (blue). Spectra were normalized to optical density.*

The DSC measurement of a bulk sample did not reveal any surprises. Melting occurs between 54 - 69 °C with an endothermic peak at 65 °C, upon cooling exothermic freezing starts at 38 °C and terminates at 17 °C displaying an exothermic peak at 25 °C. Compared to the pure PPO strand **MB203b** of same length, melting and freezing peaks are both shifted by two degrees to lower temperatures and the ranges are narrower. No additional signals indicating rearrangements in the bulk or melt were observed in the temperature range of -20 °C to 100 °C.

3.6 References

[1] H.-A. Klok, S. Lecommandoux, *Adv. Mater.* **2001**, *13*, 1217-1229.
[2] J. J. L. M. Cornelissen, A. E. Rowan, R. J. M. Nolte, N. A. J. M. Sommerdijk, *Chem. Rev.* **2001**, *101*, 4039-4070.
[3] M. Muthukumar, C. K. Ober, E. L. Thomas, *Science* **1997**, *277*, 1225-1232.
[4] F. S. Bates, *Science* **1991**, *251*, 898-905.
[5] M. Lee, B.-K. Cho, W.-C. Zin, *Chem. Rev.* **2001**, *101*, 3869-3892.
[6] G. W. M. Vandermeulen, H.-A. Klok, *Macromol. Biosci.* **2004**, *4*, 383-398.
[7] D. T. McQuade, A. E. Pullen, T. M. Swager, *Chem. Rev.* **2000**, *100*, 2537-2574.
[8] S.-H. Yu, H. Cölfen, *J. Mater. Chem.* **2004**, *14*, 2124-2147.
[9] M. A. Balbo Block, S. Hecht, *Angew. Chem. Int. Ed.* **2005**, *44*, 6986-6989.
[10] H.-A. Klok, *J. Polym. Sci., Part A: Polym. Chem.* **2005**, *43*, 1-17.
[11] B. M. Discher, Y.-Y. Won, D. S. Ege, J. C. M. Lee, F. S. Bates, D. E. Discher, D. A. Hammer, *Science* **1999**, *284*, 1143-1146.
[12] J. Ruokolainen, R. Mäkinen, M. Torkkeli, T. Mäkelä, R. Serimaa, G. t. Brinke, O. Ikkala, *Science* **1998**, *280*, 557-560.
[13] X. Kong, S. A. Jenekhe, *Macromolecules* **2004**, *37*, 8180-8183.
[14] M. J. Mio, L. C. Kopel, J. B. Braun, T. L. Gadzikwa, K. L. Hull, R. G. Brisbois, C. J. Markworth, P. A. Grieco, *Org. Lett.* **2002**, *4*, 3199-3202.
[15] U. H. F. Bunz, *Chem. Rev.* **2000**, *100*, 1605-1644.
[16] For an example, see: I. C. Stewart, C. C. Lee, R. G. Bergman, F. D. Toste, *J. Am. Chem. Soc.* **2005**, *127*, 17616-17617.
[17] For an example, see: V. Boucard, P. Dumas, P. Sigwalt, D. Rucar, *Makromol. Chem.* **1993**, *194*, 1015-1025.
[18] M. Cesari, G. Perego, W. Marconi, *Makromol. Chem.* **1966**, *94*, 194-204.
[19] O. Rexin, R. Mulhaupt, *J. Polym. Sci., Part A: Polym. Chem.* **2002**, *40*, 864-873.
[20] N. Ueyama, T. Araki, H. Tani, *Macromolecules* **1974**, *7*, 153-160.
[21] N. Oguni, S. Watanabe, M. Maki, H. Tani, *Macromolecules* **1973**, *6*, 195-199.
[22] T. Aida, S. Inoue, *Macromolecules* **1981**, *14*, 1166-1169.
[23] Y. Watanabe, T. Aida, S. Inoue, *Macromolecules* **1990**, *23*, 2612-2617.
[24] H. Sugimoto, C. Kawamura, M. Kuroki, T. Aida, S. Inoue, *Macromolecules* **1994**, *27*, 2013-2018.
[25] D. Chakraborty, A. Rodriguez, E. Y. X. Chen, *Macromolecules* **2003**, *36*, 5470-5481.
[26] W. Kuran, *Prog. Polym. Sci.* **1998**, *23*, 919-992.
[27] K. L. Peretti, H. Ajiro, C. T. Cohen, E. B. Lobkovsky, G. W. Coates, *J. Am. Chem. Soc.* **2005**, *127*, 11566-11567.
[28] C. Billouard, S. Carlotti, P. Desbois, A. Deffieux, *Macromolecules* **2004**, *37*, 4038-4043.
[29] C. C. Price, M. Osgan, *J. Am. Chem. Soc.* **1956**, *78*, 4787-4792.
[30] For optical rotation, see: Y. Kumata, J. Furukawa, T. Fueno, *Bull. Chem. Soc. Jpn.* **1970**, *43*, 3663-3666.
[31] For circular dichroism, see: T. Hirano, A. Sato, T. Tsuruta, W. C. Johnson, Jr., *J. Polym. Sci., Polym. Phys. Ed.* **1979**, *17*, 1601-1609.
[32] M. H. Chisholm, D. Navarro-Llobet, *Macromolecules* **2002**, *35*, 2389-2392.
[33] B. Antelmann, M. H. Chisholm, S. S. Iyer, J. C. Huffman, D. Navarro-Llobet, M. Pagel, W. J. Simonsick, W. Zhong, *Macromolecules* **2001**, *34*, 3159-3175.
[34] C. Harlan, A. Bott, B. Wu, R. Lenz, A. Barron, *Chem. Commun.* **1997**, 2183-2184.

[35] B. Rivas, B. Barria, G. Canessa, F. Rabagliati, J. Preston, *Macromolecules* **1996**, *29*, 4449-4452.
[36] K. Sakurai, G. Amador, T. Takahashi, *Polymer* **1998**, *39*, 4089-4094.
[37] R. Saint-Loup, J. Robin, *Macromol. Chem. Phys.* **2005**, *206*, 1190-1198.
[38] J.-H. Ryu, N.-K. Oh, W.-C. Zin, M. Lee, *J. Am. Chem. Soc.* **2004**, *126*, 3551-3558.
[39] V. Francke, H. J. Räder, Y. Geerts, K. Müllen, *Macromol. Rapid Commun.* **1998**, *19*, 275-281.
[40] W. Y. Huang, S. Matsuoka, T. K. Kwei, Y. Okamoto, *Macromolecules* **2001**, *34*, 7809-7816.
[41] P. Leclere, A. Calderone, D. Marsitzky, V. Francke, Y. Geerts, K. Müllen, J.-L. Bredas, R. Lazzaroni, *Adv. Mater.* **2000**, *12*, 1042-1046.
[42] C. J. Yang, M. Pinto, K. Schanze, W. Tan, *Angew. Chem. Int. Ed.* **2005**, *44*, 2572-2576.
[43] M. Bochmann, K. Kelly, *J. Polym. Sci., Part A: Polym. Chem.* **1992**, *30*, 2503-2510.
[44] O. Lavastre, L. Ollivier, P. H. Dixneuf, S. Sibandhit, *Tetrahedron* **1996**, *52*, 5495-5504.
[45] A. Pelter, D. E. Jones, *J. Chem. Soc., Perkin Trans. 1* **2000**, 2289-2294.
[46] G. Voskerician, C. Weder, *Adv. Polym. Sci.* **2005**, *177*, 209-248.
[47] V. A. Solomin, W. Heitz, *Macromol. Chem. Phys.* **1994**, *195*, 303-314.
[48] U. H. F. Bunz, V. Enkelmann, L. Kloppenburg, D. Jones, K. D. Shimizu, J. B. Claridge, H.-C. zur Loye, G. Lieser, *Chem. Mater.* **1999**, *11*, 1416-1424.
[49] S. Anderson, *Chem. Eur. J.* **2001**, *7*, 4706-4714.
[50] G. N. Tew, M. U. Pralle, S. I. Stupp, *J. Am. Chem. Soc.* **1999**, *121*, 9852-9866.
[51] E. Stanley, M. Litt, *J. Polym. Sci.* **1960**, *43*, 453-458.
[52] J. Israelachvili, *Intermolecular and Surface Forces*, 3 ed., Academic Press, London, **2003**.
[53] D. L. Trumbo, C. S. Marvel, *J. Polym. Sci., Part A: Polym. Chem.* **1986**, *24*, 2311-2326.
[54] S. Lahiri, J. L. Thompson, J. S. Moore, *J. Am. Chem. Soc.* **2000**, *122*, 11315-11319.
[55] C. A. Hunter, K. R. Lawson, J. Perkins, C. J. Urch, *J. Chem. Soc., Perkin Trans. 2* **2001**, 651-669.
[56] J. C. Nelson, J. G. Saven, J. S. Moore, P. G. Wolynes, *Science* **1997**, *277*, 1793-1796.
[57] M. J. Mio, R. B. Prince, J. S. Moore, C. Kuebel, D. C. Martin, *J. Am. Chem. Soc.* **2000**, *122*, 6134-6135.
[58] C. Breen, T. Deng, T. Breiner, E. Thomas, T. Swager, *J. Am. Chem. Soc.* **2003**, *125*, 9942-9943.
[59] Y. Jiang, D. Perahia, Y. Wang, H. F. Bunz Uwe, *Macromolecules* **2006**, *Asap*.
[60] Compound was synthesized and kindly provided by Christian Kaiser.
[61] J. Moore, S. Stupp, *Macromolecules* **1990**, *23*, 65-70.